energies

MDPI

Review

Semitransparent Perovskite Solar Cells for Building Integrated Photovoltaics: Recent Advances

Kalavala Shivaprakash Srivishnu [1,2], Prasutha Rani Markapudi [3], Senthilarasu Sundaram [3] and Lingamallu Giribabu [1,2,*]

[1] Polymers & Functional Materials Division, CSIR-Indian Institute of Chemical Technology, Uppal Road, Tarnaka, Hyderabad 500007, India
[2] Academy of Scientific and Innovative Research (AcSIR), Kamala Nehru Nagar, Ghaziabad 201002, India
[3] School of Computing, Engineering and the Built Environment, Merchiston Campus, Edinburgh Napier University, Edinburgh EH10 5DT, UK
* Correspondence: giribabu@iict.res.in

Abstract: Perovskite solar cells technology is one of the most advanced and fascinating technologies in the field of photovoltaics due to its low-cost processing and delivering efficient power conversion efficiencies. The ability to become transparent is another prolific property of the perovskite solar cells, which this property has been tried to be exploited in recent times by researchers to serve the environmental and energy needs of human beings. Using this transparency and enabling semitransparent perovskite solar cells (ST-PSCs) to be placed on the windows and rooftops of buildings will reduce room temperature along with fulfilling certain requirements of power needs. This review pays attention to the recent developments in the semitransparent perovskite solar cells from the perspective of the structure of ST PSCs, electrodes and others.

Keywords: building integrated photovoltaics; perovskites; flexible; semitransparent; nano

Citation: Srivishnu, K.S.; Markapudi, P.R.; Sundaram, S.; Giribabu, L. Semitransparent Perovskite Solar Cells for Building Integrated Photovoltaics: Recent Advances. *Energies* **2023**, *16*, 889. https://doi.org/10.3390/en16020889

Received: 7 December 2022
Revised: 26 December 2022
Accepted: 6 January 2023
Published: 12 January 2023

1. Introduction

The International Energy Agency (IEA) reported that buildings consume greater than 30% of the energy produced globally; with the population growth increase in household size, advancement in cooking and electrical appliances, and changes in the lifestyle of the people, it is further expected to increase two-fold by 2050 [1]. Along with the consumption of energy, these buildings will be solely responsible for the emission of carbon dioxide by 30% globally [2]. Generally, the amount of solar radiation entering the room increases significantly during a sunny day and thus, the consumption of the energy in the room increases with the usage of the air-conditioner and rooftop fans. This is a serious issue in buildings with high window-to-wall ratios [3]. Hence, the reduction of energy consumption in buildings that are currently using fossil fuels [4] or other non-renewable energy sources is of great interest. On the other hand, an effective approach will also be the proper management of solar radiation entering the buildings, which helps to decrease cooling loads and the spending of energy on air conditioning [5]. One such alternative to the generation of energy is by harvesting solar energy [6,7]. Generating power using PV technology could displace the energy generated by fossil fuels [8], with over 600 GW of PV installed by 2020, with an expected increase of another 500 GW by the end of 2023 [9]. PV's integration into building architecture has opportunities along with challenges [10,11]. The integration of PV into windows, shades and blinds can reduce the cooling loads significantly [12]. The Integration of PV modules into the building parts, such as windows and rooftops, is known as Building Integrated Photovoltaics (BIPV), and these can replace traditional windows entirely (Figure 1) [13]. These BIPV windows can control the solar radiation entering the room, which further reduces the power consumption of the cooling aids [14], which traditional windows cannot do. Moreover, BIPV windows mitigate the light

glare from windows [15]. With over 70% of market distribution in all segments, including roof and facade applications, crystalline silicon PV dominates the current global BiPV market (Figure 2) [16]. It is also expected to follow a similar trend for several more coming years, predominantly since it is predicted that the price of crystalline silicon (c-Si) solar cells price will drop in the future [17]. Glass is the structural backbone of buildings [18] so it can be expected that solar cells can be directly developed on the glass as the current world moves in the direction of nearly zero-energy buildings with the advancement of smart technologies and the help of photovoltaics [19]. Even other PV technologies, such as thin film technology consisting of copper indium gallium selenide (CIGS), copper zinc tin sulfide (CZTS), organic photovoltaics (OPVs), and emerging Perovskite Solar Cells (PSCs) are complementary to BIPV [20]. The advancement of these solar technologies enhances flexibility, and the products are lightweight with customisable sizes and distinguishable colours [21].

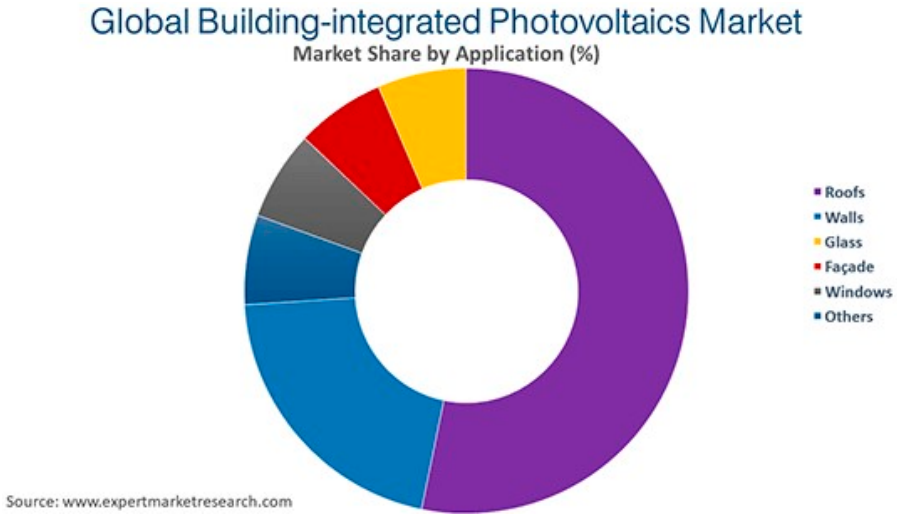

Figure 1. Market segmentation of global building-integrated photovoltaics [13].

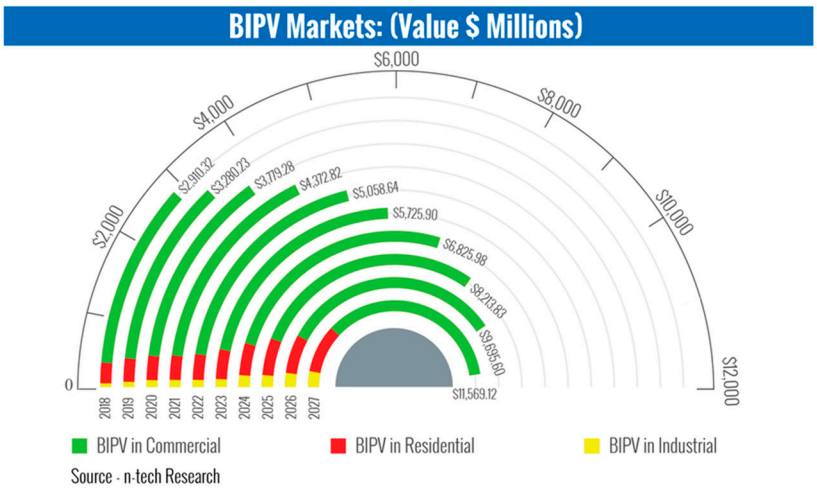

Figure 2. The market value of BIPV [16].

Though the current market is conquered by the highly efficient c-Si modules, they are not perfect for BIPV applications because of their poor and inadequate aesthetic appearances, as they are opaque [22] and rigid in nature, even though they are economical and highly stable [23]. This has paved the way for exploring different light-absorbing materials for the expansion of the BIPV market [24]. For BIPV applications, CIGS-based thin film technology gives a new perspective in which it showed power conversion efficiencies (PCE)

of over 23% for lab scale cells and for modules yielding over 19% PCE [25]. With several advantages, such as strong light-harvesting capacity, high stability and the capability to fabricate on the curved surface, CIGS PV is presently the leading thin film solar technology [26]. However, these technologies' major drawbacks arise from insufficient indium and expensive fabrication cost [27]. CZTS is another thin film candidate; although it does not have rare earth metal indium, it endures from low power conversion efficiencies [28]. Along with thin film technologies, OPV and dye-sensitised solar cells have been studied for decades and can provide visually attractive configurations with high transparency [29]. In OPV modules, these technologies enable tuneable transparency and a range of colours from blue to dark brown [30]. The main advantage of the OPV lies in its minimum fabrication cost, which involves roll-to-roll printing, leading to easy fabrication [31]. The barrier of this technology is its low module conversion efficiency (<9%) and operating life, which has not yet been reached by the standard set of silicon-based PV modules [32].

2. Dye-Sensitised Solar Cells

In contrast, DSSC is a photovoltaic technology based on a photo-electrochemical system, which imitates photosynthesis, where the photoactive sensitisers are attached to a titanium dioxide transport layer which absorbs photons and produces charges [33]. These solar cells can be tuned with a wide range of colours [34]. DSSCs are particularly suitable for portable electronic applications which use smaller modules but are not that effective for terrestrial power generations, which require bigger modules [35]. Due to their excellent performance under indoor light conditions, they are attractive for portable electronics when compared to other solar cell technologies [36]. Even in cases of greenhouse applications, DSSCs play an important role [37] when compared to other technologies, as the colours of the DSSCs can be tuned by varying the dye [38]. Thus, these dye solar cells can act as plant growth regulators or photo-selective coverings by changing the light spectrum, which helps in optimising plant growth [39]. Transparency in DSSCs can be adjusted, which can minimise the negative impacts on plant growth which is not possible in Si cells which are opaque [40]. Besides generating electricity, DSSCs can be integrated into smart farming in rural areas [41].

It is essential to understand the degradation mechanisms in DSSCs to improve their lifetime [42]. The factors included in the degradation of DSSCs are leaking of the electrolyte, decrease in the I3-concentration, which results in the change from yellow colour to colourless liquid, and the instability of Pt in the electrolyte to avoid this liquid electrolyte should be turned to solid electrolyte which was first reported by Bach et al. using 2,2′,7,7′-tetrakis-(N,N-di-p-methoxyphenylamine)9,9′-spirobifluorene (spiro-OMeTAD) as a hole transport material (HTM) [43]. Thereafter the spiro-OMeTAD was started to be used as HTM for various technologies, including perovskite solar cells, which got an efficiency of more than 25% [44]. The degradation of counter-electrode is a major problem where Pt has commonly used catalyst for coating electrodes because of its impressive electrocatalytic performance and high electric conductivity [45]. However, Pt coatings are not stable and can corrode, which leads to the formation of PtI4; moreover, Pt is rare there are several alternatives that have been studied and replaced [46]. The other issue is improper sealing which leads to electrolyte leakage and entry of moisture which results in the degradation of DSSCs [47]. The main challenge is maintaining cell efficiency as the DSSC module is constructed with many interconnected cells in parallel or series architecture [48]. By adopting W-type interconnection, the fabrication of the DSSCs module showed an efficiency of 8.2% [49]. However, there is still a gap between application obligation and reported performance [50]. Similarly to OPVs, these solar cells are also limited owing to their lesser efficiencies which are less than 9% at the module levels, and there is a need for improvement for stability which requires much engineering effort [51].

3. Perovskite Solar Cells

Perovskite Solar Cells (PSCs) have been interesting topics among researchers globally due to their high-power conversion efficiency (PCE), low-cost materials and simple fabrication procedure [52]. The crystal structure of the perovskite solar cells is similar to Calcium Titanate ($CaTiO_3$), and a formula with ABX_3 [A=FA ($NH_2CH{=}NH_2$), MA (CH_3NH_3); B=Pb_2; X=Cl, Br or I] (where X is a halide) [53] Halide perovskites are of two types they are alkali halide-based perovskite has monovalent alkali cation (A) as (Cs, Rb, K, Na and Li), divalent cation (B) as (Pb, Sn, Ge) and halogen X as (Cl, Br, I, F) and organic-inorganic halide based perovskites have organic monovalent cation (A) as CH_3NH_3,$CH_3CH_2NH_3$,NH_2CHNH_2 [54]. Perovskite material has exceptional optical and electrical properties, which make them advanced photovoltaic technology. They are high absorption coefficient, tunable band gap, long diffusion length, low carrier recombination loss and high carrier mobility [55]. Due to these properties, it is possible to fabricate semi-transparent solar cells where some part of the light is absorbed by the light-harvesting layer, and some of it can pass through cells [56]. By tuning the band gap, it is achievable to control the transparency by making a thin perovskite layer [57].

The first reported photovoltaic device is based on lead halide perovskite material with an efficiency of 2.2% by Miyasaka using $CH_3NH_3PbBr_3$ and by replacing bromine with iodine achieved an efficiency of 3.8% [58]. Using spiro-MeOTAD as hole-transporting material achieved an efficiency of 9.7% in the first solid perovskite solar cells fabricated by Kim et al. in 2012 [59]. Later, PSCs reached a power conversion efficiency of 23% by engineering the thin film deposition and the perovskite composition method [60]. Recently, the power conversion efficiency of PSCs reached 25.2%, which is found in the NREL PV chart [61]. The PCE of perovskite solar cells has enhanced quickly from 3.8% to 25.2% within a decade [62]. So, these are considered to replace the most used silicon-based solar cells. Despite the emerging results of perovskite solar cells with high power conversion efficiency and low-cost fabrication, these devices still face a lot of challenges which include toxicity of lead and short-term stability [63]. Researchers are showing curiosity in developing lead-free perovskites with high stability and low toxicity. The layers in the perovskite solar cells are transparent conductive oxide (TCO), an electron transport layer (ETL), a light absorbing perovskite layer, a hole transporting layer (HTL) and a metal electrode [64]. Among these benefits, the fabrication process of perovskite is based on the solution process, which allows a variety of deposition techniques which are screen printing, spin coating and evaporation [65]. Flexible electronics have been attractive due to their unique properties, which are lightweight and high flexibility [66]. In 2019, flexible perovskite solar cells were progressing with improvements in stability and device efficiency. Huang and his group achieved a record efficiency of 19.5% in single-junction perovskite solar cells [67]. Palmstorm and his co-workers fabricated tandem flexible perovskite solar cells with an efficiency of more than 21% [68].

The optoelectronic properties such as high absorption coefficient (10^5 cm^{-1}), high charge carrier mobilities (>10 cm^2 V^{-1} s^{-1}), long carrier diffusion length (>1 μm), small tunable bandgap (1.2–3.0 eV) and exciton binding energy (≈20 meV) with compositional engineering and enabling various crystallisation methods which are vapour deposition and solution process [69] PSCs are suitable for BIPV applications for their following properties:

3.1. High Optical Absorption Coefficient

Even with a thin absorbing layer, efficient light harvesting is guaranteed as perovskites have high absorption coefficients, which offer high transparency that is necessary for BIPV applications [70]. The absorption coefficient is critical for light-absorbing materials, but it is not the exact parameter in the balance limit inferences for the maximum PCE of solar cells [71]. The maximum efficiencies of different light absorbers as a function of absorber thickness suggest a close correlation to the absorption coefficient of the active semiconductor. In thin-film technologies, perovskite PV($CH_3NH_3PbI_3$) shows much higher PCE than CIS,

GaAs and CZTS at any thickness. To achieve high power conversion efficiencies, the optical absorption in perovskites allows the use of ultrathin absorber layers (500 nm) [72].

3.2. Bandgap Tunability

The capability to tune the optical bandgap in perovskites is one of the principally promising properties for various optoelectronic applications. The easiest and straight process is through compositional mixing. Formamidinium (FA), methylammonium (MA) and caesium (Cs) are mostly used as monovalent A-site cations for PSCs [73]. The mostly known halide perovskite is $MAPbI_3$, with a bandgap of nearly 1.57 eV. At present, compositional engineering in perovskite absorbers is followed from the point-of-view of bandgap tenability and as an approach for improving stability, reproducing process and high PCE. Bandgap and structural device tunability suggest the fabrication of colourful PSCs [74].

3.3. Versatile and Scalable Fabrication Processes

Deposition of light absorbing layer uniformly on a substrate is the key factor to achieving high PSCs of more than 25%. The perovskite precursor solution is directly spin-coated over the substrate, resulting in pinholes formation and thickness, which is uncontrollable and morphology. The antisolvents where the perovskite is insoluble are dropped onto the substrate while spinning was the key to accomplishing PSCs with more than 20% efficiency [75]. This accelerates heterogeneous nucleation and leads to supersaturation, improvement in morphology, uniformity, and pinhole-free perovskite layer. The spin-coating method is not an ideal technique for PSCs due to material wastage. In blade-coating, [76] slot-die coating [77] and roll-to-roll printing, [78] the precursor solution is transferred to a substrate as a wet film which is crystallised by air-knife and heating. The precursor properties such as viscosity, concentration, volatility of the ink and substrate wetness play an important role in perovskite film formation.

3.4. Excellent Mechanical and Flexible Properties

High durability is one more essential requirement for BIPV because the solar panels would be subjected to erratic weather conditions. PSCs have displayed outstanding mechanical characteristics, including great bending resistance and strong pressure endurance. In 2015 Park et al. demonstrated that perovskites had a very low elastic modulus of 13.5 GPa and yield stress of 17.3 MPa, which is thought to have contributed to their great flexibility and endurance [79]. With flexible PSCs obtaining PCEs exceeding 20% from solution process technology and 19% from the co-evaporation process, the sector has expanded quickly [80]. Recently, Finkenauer et al. created an interpenetrating composite that allows mechanical self-healing in perovskite by incorporating a self-healing polymer into a thin layer of polycrystalline perovskite. In addition to having high durability, mechanical robustness, and outstanding stability, self-healing PSCs with PCEs > 13% also preserve 94% of their early efficiencies after 3000 bending cycles [81]. Perovskites may develop over both rigid and flexible surfaces due to low crystallisation temperatures.

4. Materials Design Strategy for Perovskite Solar Cells to Suit BiPV Applications: Each Component of the Perovskite Device Has Been Redesigned and Is Suitable for BIPV Applications as Discussed in the following Sections

4.1. Ultrathin Semitransparent Perovskite Solar Cells (ST-PSCs)

The transparency of the PSC device, decreased by the perovskite, turns out to be the game changer. When the thickness of the perovskite is less than the penetration depth, then the ultrathin absorber can transmit visible light. One such method to produce an ultrathin PSC is a spin coating with low concentration, and co-evaporation is a suggested technique. In this aspect, Enrico and the group developed PSCs with thin layers of perovskite ranging in size from 54 nm to 289 nm, for which they achieved PCE of 4.6 and 11.7%, respectively. They increased the perovskite film thickness from around 50 nm to 300 nm by raising the precursor concentration gradually. The grain size of perovskite, which was seen from the SEM image, was found to be smaller in thin films (100 nm) than in 300 nm film [82].

Although pinholes were observed, these films appeared to be continuous and homogenous at every thickness in which they were assessed [83]. With 7% average transparency (AVT), the semitransparent devices developed using different thicknesses showed a record PCE of 13.6%. These results inspire in fabricating the solar cells with high transparency and efficiency for building-integrated PVs (Figures 3 and 4). Im et al. reported that the charge extraction properties of the PSC were also influenced by the thickness of b-MoO_3 due to its limited conductivity. A thin layer of MoO_3 (≈1 nm) was coated over the spiro-OMeTAD, which produced lesser sheet resistance and better efficiencies [84]. Studies also showed that the usage of additives in the perovskite solution could also increase the stability of the PSCs. In the precursor solution of perovskite, HI additives were added, which helped in achieving an ultrathin and uniform film by using the spin-coating technique. By controlling the thickness of MAPbI3, the AVT was controlled from 17.3% to 6.3%.

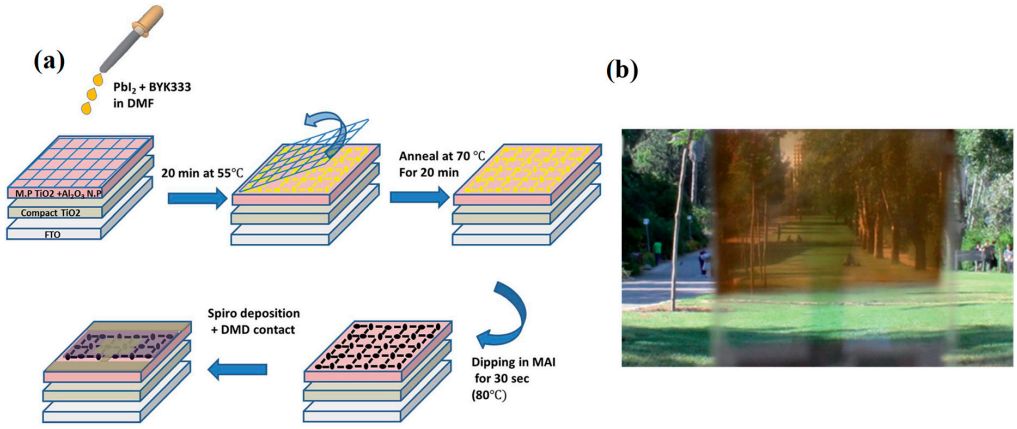

Figure 3. (**a**) A two-step deposition process used to create a semitransparent perovskite solar cell. The PbI_2 grid is first created and annealed, after which the entire electrode is submerged in the MAI solution to create the $MAPbI_3$ grid. The hole transport material (HTM) layer is covered with an evaporated dielectric-metal-dielectric contact during the final stage. (**b**) Semitransparent device. [83].

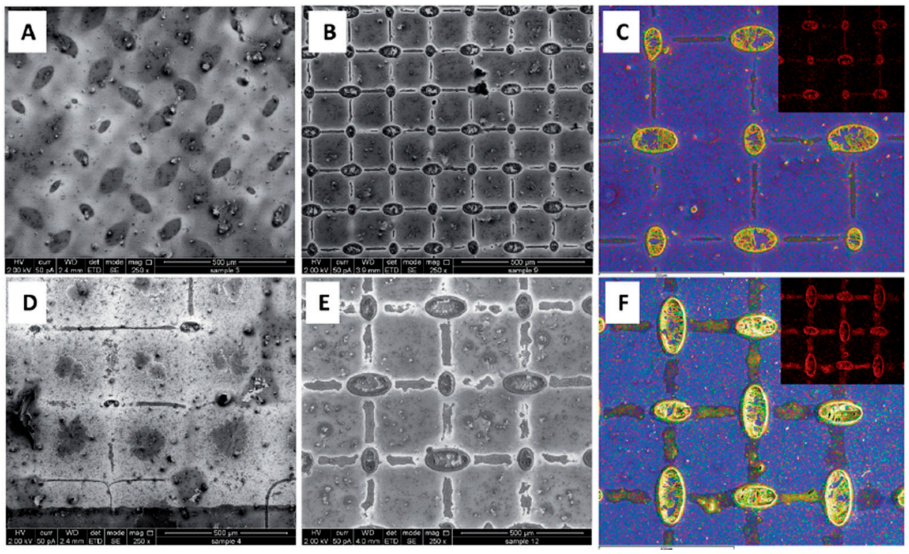

Figure 4. HRSEM images for 0.2 M PbI_2 grid obtained using: (**A**) 85 µm size of mesh before annealing. (**B**) With annealing, mesh size. (**C**) PbI_2 chemical mapping (A grid developed during annealing using a mesh size of 85 µm is coloured yellow for the Pb metal and red for the inset I). (**D**) 240 µm without annealing mesh. (**E**) 240 µm mesh size with annealing (**F**) PbI_2 chemical mapping (A grid developed during annealing using a mesh size of 240 µm is coloured yellow for the Pb metal and red for inset I). When the grid was formed, the temperature was 70 °C for samples B, C, E and F. [83].

4.2. Microstructured ST-PSCs

Further, semitransparency was achieved by creating transparent regions by using microstructures perovskite devices. By using de-wetting techniques or microscale templates, these microstructures ST-PSCs can be created. By controlling the perovskite region, this structure can be used to create solar cells which are neutral-coloured. In the fabrication of ST solar cells, ordered microstructures have also been recommended. By usage of the polystyrene microsphere method, the microporous type was developed by Yong Su and co-workers [85]. By modifying the polystyrene (PS) diameters precursor solution, the AVT was found to be about 20% to 45% after the tuning. Developed semitransparent type PSC demonstrates a noteworthy PCE of around 11.7% and AVT of 36.5%. This can also be used in tandem solar cells and BiPV. It is understood that microporous structures help PSCs to achieve high PCE along with other benefits, such as reducing the recombination. One more study found that changing the concentration of perovskite in the solution and the mesh openings could control the transparency of mesh-structured solar cells. The device has 5% efficiency and approximately 20% transparency. The perovskite grid is placed on a mesoporous TiO_2 layer, and then HTM is deposited. The transparencies were adjusted by increasing the assembly concentration solution from 7.5 to 20% by weight. Because of the ability to calculate the specific coverage of the perovskite grid in the active area, transparency control via perovskite grid formation is far more advantageous. Solar cells made with gold contacts have an efficiency of 8% and average transparency of 26%, while devices made of $MoO_3/Au/MoO_3$ have a PCE of about 5.5%. The mesh-assisted deposition was used to create the PSCs [86]. Snaith et al. reported template microstructural ST-PSCs as a reason to improve open-circuit voltage and fill factor in comparison to unstructured partly de-wet perovskite thin film. The device has a PCE of 9.5% and an AVT of 37% [87]. Microstructured PSC has been disclosed in another report. The devices used a unique transparent cathode, allowing the fabrication of neutral-coloured semitransparent solar cells. The devices are more than 5% efficient for a 30% average visible transparency.

4.3. Nanostructured ST-PSCs

When considering device performance, the structure is critical. Therefore, one cannot overlook the significance of device structure. The mixed structure with oxide materials has an efficiency of 10.06% and an AVT of about 27% [88]. The $MAPbI_3$-xClx-NiO composite with inter-facial layers of Al_2O_3 and NiO is critical for improving carrier extraction and transport. Additionally, the impenetrable and sufficiently thicker but semitransparent $MAPbI_3$-xClx-metal oxides composite layer improves light harvesting and air stability [89]. The devices demonstrated exceptional stability without encapsulation over 270 days, with the device retaining approximately 98% of its preliminary efficiency under ambient conditions. Chao Li et al. reported improved transparency across the visible wavelength range created by using a low-temperature PCBM-assisted growth method. This technique is responsible for the formation of perovskite-PCBM hybrid materials at grain boundaries, as observed by EELS mapping as well as proved by steady-state photoluminescence (PL) spectra and X-ray photoelectron spectroscopy (XPS) transient photocurrent (TP) measurements, With an AVT of 18%, efficiency was reported to be 9.1% [90] These findings point to a simple method for producing high efficiency, of more solar cells for use in building integrated PVs (Figure 5).

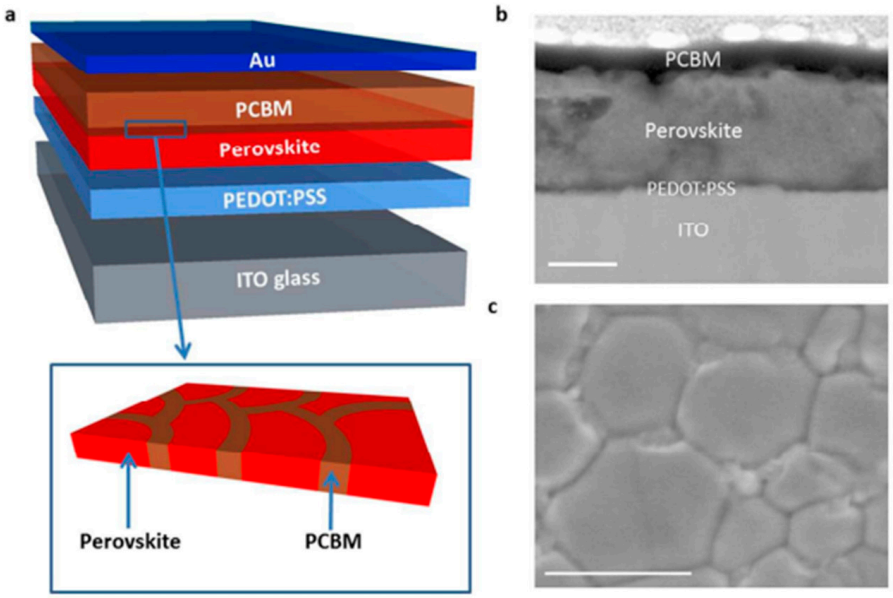

Figure 5. Perovskite solar cell structure: (**a**) schematic representation of the perovskite solar cell's architecture; the zoomed-in diagram shows the hybrid material created. (**b**) Perovskite solar cells were grown with PCMB assistance and TEM cross-section view. Scale bar: 100 nm. (**c**) The view from above SEM image of a perovskite film that was grown using a CB-assisted process in conditions similar to those for PCMB-assisted growth. Scale bar: 1 µm [90].

With 12.32% PCE, there was another semitransparent report with extremely thin around 100 nm perovskite film with dual scaffolds [91]. By using aluminium oxide as a scaffold layer, Kwon et al. developed a highly efficient ST nanostructured PSC [92]. In another report on perovskite film, Nano pillars in parallel were discovered, which also helps in the development of easy making of semitransparent devices. By controlling the size of the pore in the perovskite film, the neutral colour of the device can be achieved. The device achieved around 9.6% of PCE with 33.4% AVT. Some other group studies the dynamics of charge carriers and recombination. They examine the effects of the 1-D nanostructure CH3NH3PbI3-xClx on these processes. It was discovered that 1-D perovskite outperforms its planar counterpart in terms of charge transport/extraction, bulk resistance, and defect density [93]. A p-type Nickel oxide nanoparticles were deposited on the perovskite film to avoid the damage caused during sputtering on the transparent conducting oxides. Noh et al. showed that this acts as both a hole transporting and buffer layer. Even under high temperatures and harsh sputtering conditions, these NiOx-based ST-PSCs showed high durability, producing high-quality transparent electrodes. Enhanced PCE of 19.5% was achieved by this ST-PSC device, which is increased when compared to an opaque device, which showed 19.2% when ITO was sputtered on a transparent top electrode. The device retained 90% of its initial PCE even after 1000 h, which displayed high storage stability. By controlling the molar concentration of perovskite film, an ST-PSC device was fabricated with 12.8% PCE, which showed 30.3% high AVT was showed by Jun Hong et al., and they believed the device architecture of n-type oxide/perovskite halide/p-type oxide shows a basis for the better performance and commercialisation of ST-PSCs [94].

Despite the fact that numerous studies have demonstrated how small molecule additives can enhance ST-PSC properties, this study is the first to employ relatively enormous microgel particle (MGs) additives such as poly(N-isopropylacrylamide) polymer colloids. Unusually, these MGs formed highly ordered particle arrays in 2D non-close packed structures when deposited. Surprisingly, the perovskite layer's arrays reflect this morphology. The MGs in the nanopores block shunts. The themes-based device achieved an AVT of 25.3% with a PCE of 11.64%. For an ideal system, the average light utilisation efficiency (LUE) is 2.60%, higher than that without MG and a control system and higher than the 2.50%

threshold necessary for application in theory. The Pb^{2+} ions are bound by the MGs, which passivates the perovskite film. According to simulation data from the finite difference time domain (FDTD), MGs cause the AVTs of the films to increase when compared to uniform MG-free films. It is suggested that the MGs function as nanoscale optical windows. The new method developed by Brian and his team for making ST-PSCs produces perovskite films with 2D nanopore arrays in a single step, improving PCEs and AVTs and possibly speeding up the development of ST-PSC applications in the future [95].

4.4. Transparent Electrodes

In terms of device transparency, in order to develop semitransparent PSCs, both the cathode and anode should be transparent. Normally, electrodes have a direct impact on the properties of semitransparent cells. Electrodes which are transparent are mostly determined by the device's processing and optical properties, as well as its electrical conductivity. In the case of organic solar cells, transparent electrodes are usually made of transparent conductive oxides (TCO), such as Indium tin oxide (ITO), which must be manufactured at high temperatures (Figure 6) [96]. As a result, innumerable materials with required transparency and conductivity have been introduced to the semitransparent devices, such as Aluminium doped Zinc oxides, Fluorine-doped tin oxides and indium tin oxides. Conductivity and transparency, as listed below, have been introduced into ST-PSCs as transparent electrodes [97–99].

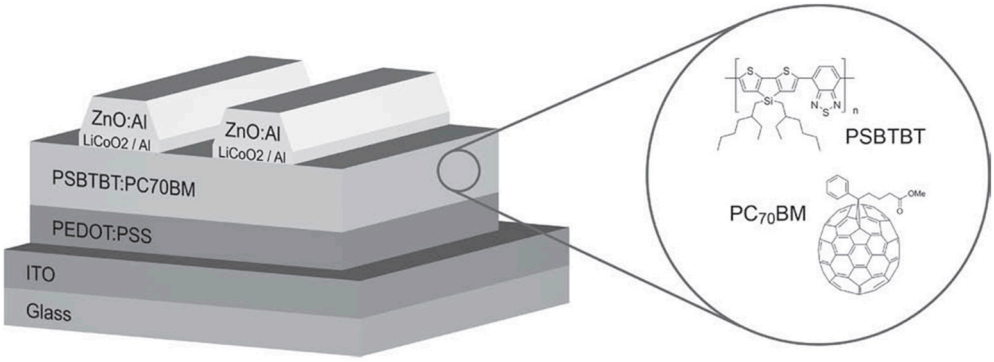

Figure 6. Left: Semitransparent photovoltaic device architecture consists of a $LiCoO_2$/Al interfacial layer, a transparent cathode made of sputtered ZnO:Al, and an active layer made of PSBTBT:PC70BM. Right: Co-polymer PSBTBT and acceptor fullerene PC70BM's molecular structure [96].

However, due to its outstanding optoelectronic properties and commercial availability, the most commonly used electrode for opaque and ST devices is ITO. Even though owing to commercial availability, ITO is good for transparency, it does suffer from a few drawbacks, such as they are inconsistent for moving electronic devices because of its excessive mechanical brittleness. Even when compared with the cost, electroplating, sputtering and pulsed laser deposition high cost is involved [100]. More likely, in future, the oxide-based electrodes for transparency will include amorphous, easily depositional materials. Amorphous ITO derivatives, as well as InSiO, [101] InZnAlO, [102] and $ZnSnO_3$, [103] maintain moderate conductivity and are currently being tested as capable transparent electrodes in flexible devices.

4.5. Transparent Conductive Oxide

To promote transparent electrodes, many efforts have been made. Given that Transparent Conductive Oxides have low resistivity and broadband transparency, it is reasonable to expect that the use of TCO electrodes on both sides will improve the transmittance and efficiency of semitransparent devices [104]. The most commonly used conductive electrodes are FTO, ITO and Al-doped zinc oxide. When compared to metallic electrodes, ITO has a higher resistivity. It is still difficult to fabricate large devices without PCE losses, even though the metallic grids help improve conductivity [105]. Because of their excellent optical and

electrical properties, Transparent Conductive Oxide electrodes are accepted widely. One of the limitations is that the perovskite film might get affected due to magnetron sputtering, which is used to deposit TCOs. To avoid sputtering, Heo et al. Laminated a device with a dry coating of PEDOT:PSS on ITO onto the wet substrate of HTL/$MAPbI_3$/TiO_2/FTO. This device with PEDOT:PSS showed an efficiency of 12.8% whereas (Figure 7). The device having FTO/TiO_2/$MAPbI_3$/PTAA with additives PEDOT:PSS/ITO exhibited around PCE of 15.8% and AVT between 6.3 to 17.3% [106].

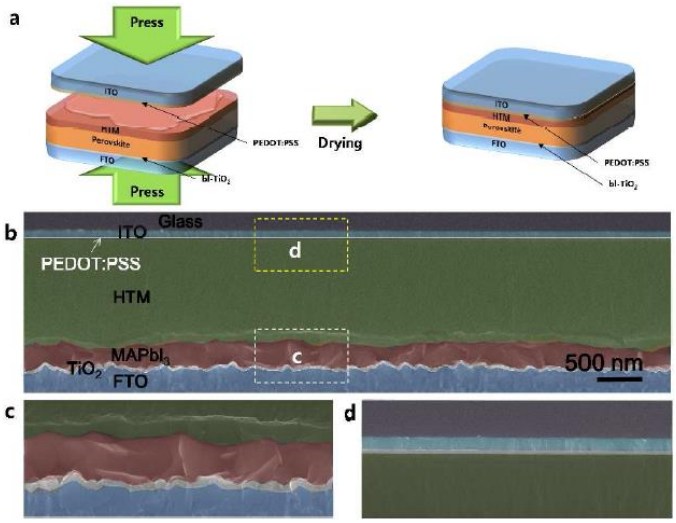

Figure 7. (**a**) MAPbI3 planar sandwich solar cell schematic illustration for device fabrication and architecture, (**b**) A typical SEM cross-sectional image of a complete sandwich cell included FTO/TiO2/MAPbI3/HTM/PEDOT:PSS/ITO/Glass and its enlarged image of (**c**) FTO/TiO2/MAPbI3/HTM part and (**d**) HTM/PEDOT:PSS/ITO/Glass part [106].

For processing conditions, light gripping materials respond quickly; the device performance can be degraded by increasing the temperature during post-annealing and sputter deposition. As a result, a barrier layer between the transparent electrodes and the perovskite absorber could provide protection during deposition [107,108]. However, a significant separation carrier could be produced by the chemical reaction of the iodine in the MoO_x layer. A protection layer of MoO_3 was applied to the spiro-OMeTAD by Fan Fu et al. before sputtering 170 nm of In_2O_3:H as a transparent electrode, which achieved a semitransparent device with AVT of 72% and PCE of 14.2% [109]. Huang et al. used two transparent plastic-coated ITO substrates as the top and bottom electrodes [110]. The pronounced advantage of this plastic substrate is that it efficiently covers the device, preventing the entry of oxygen and moisture from entering the active layer. Devices showed PCE of around 3% under standard illumination of AM 1.5, which, when compared with opaque devices, the results are similar. ITO is a fantastic material that is both transparent and conducive. However, it is fragile and cracks when bent, making it unsuitable for solar cells, which are flexible [111]. The flexible device architecture is typically based on ITO-coated flex substrates, but sadly, under severe bending conditions with a bending radius of about 4 mm, the power conversion efficiency of the ITO-based adaptable PSCs tends to be drastically reduced due to crack formation on the brittle ITO. In another report, Xa LI et al. showed highly flexible and efficient semitransparent devices with the usage of ultrathin Au and dielectric/metal/dielectric multi-layered films as the bottom and top electrodes. In the 500 to 2000 nm wavelength range, the PCE was 8.67%, and the average light transmittance was 15.94%. With a bending radius of 3.9 mm after 1000 bending cycles, the device retains 88% of its original efficiency [112]. Another study found that adding a polystyrene (PS) passivation interlayer to prevent TiO_2 PTAA from being straight contacted resulted in much better and more efficient ST-PSCs. The device with the PS layer showed an AVT of 20.9%, whereas it showed 18.9% AVT in the absence of the PS layer [113].

4.6. Metal Electrodes

If the film thickness is less than 20 nm, visible light metal films are thought to be extremely transparent, conductive, and ductile. Because metal films which are ultrathin have good flexibility and high conductivity, they are a good choice for transparent electrodes in semitransparent PSCs [114]. In solar cells, commonly used electrode materials are Ag and Al. As a result, more attention is required from researchers in order to be a better transparent electrode in device applications in all contexts. Various strategies for overcoming this situation have been reported [115,116]. The reaction of perovskite semiconductors with Ag can be avoided by the addition of a protective layer on the cathode. By using two dielectrics with high refractive indices when ultrathin metal films are sandwiched, such as $V_2O_x/Ag/V_2O_x$, ZTO/Ag/ZTO, ZnS/Ag/WO_3, $MoO_3/Ag/MoO_3$, and $MoO_3/Ag/WO_3$, their optical transmittance can be increased without losing their electrical properties (Figure 8) [117]. The inner dielectric layer helps to enhance selective charge extraction, while the outside dielectric layer alters the optical characteristics. Dangerous interference develops in the visible region when two dielectric layers are separated using a thin metal film to achieve antireflective coating effects. Top-tier potential in multiple optoelectronic devices, including various types of solar cells, photodetectors, and light-emitting diodes, has extensively examined these highly transparent conducting electrodes with numerous dielectric layers, such as MoO_3, WO_3, and V_2O_5 [118]. Y.B. Cheng et al. used this method to create a multi-layered MoO_3-Au-MoO_3 top electrode with a perovskite absorber thickness of up to 50 nm [119].

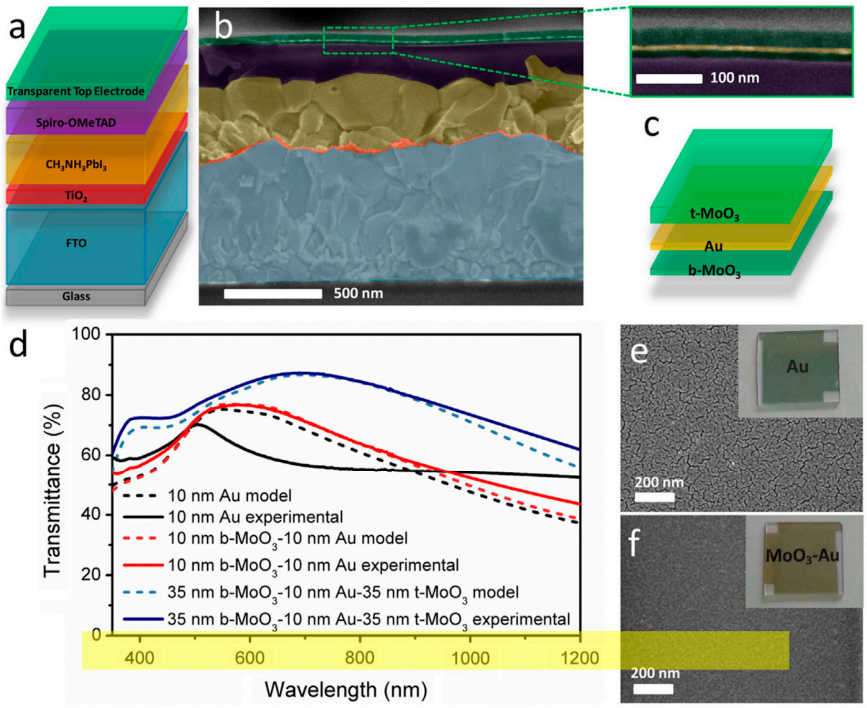

Figure 8. (**a**) Schematic representation of the PSC architecture (not to scale). (**b**) SEM image of a complete device in cross-section. (**c**) Detailed illustration of the multilayer top electrode and its structural schematic. (**d**) Experimental data (solid lines) and simulation results (shaded dashed lines) depict the transmittance of Au(black), b-MoO_3/Au (red), and b-MoO_3/Au/t-MoO_3 (blue). (**e**) Au film SEM image. (**f**) b-MoO_3/Au film SEM image. The insets show photos of the two samples [117].

Here is 3% with AVT 31%. It is demonstrated that when the thin gold film is coupled with an optimised dielectric layer, it keeps current density along with improved transparency [120]. By clinching the Au electrode with a layer of LiF and by reducing the thickness layer, significantly lower parasitic absorption in the film was achieved. Here LiF can also act as an antireflective coating and also secures the Au electrode, which helps

to adapt the division of electric field intensity in the device structure; as ETL and HTL layers, $PCBM_{60}$ and PEDTO:PSS were used respectively. This type of device could give new possible directions for the ST-PSCs [121].

4.7. AgNWs Electrodes

It is considered that multilayer and thin film electrodes are much better electrodes for obtaining better transparency. It involves the usage of high vacuum evaporation techniques to fabricate these layers. As a result, it is not well suited to the applications of large-scale or low-cost. In the alternative, with better conductivity, ease of processing, fantastic stability, and to make transparent devices, AgNWs are the suitable option [122]. However, the problem lies with AgNW electrodes, as their surface topography is quite rough. When AgNWs are used as bottom electrodes, it causes interelectrode shunting, and things get complicated further. In the literature, many other strategies have been reported to overcome these issues, such as the usage of polymer matrices such as poly-acrylates or polyvinyl alcohols, along with supplying high pressure to flatten the surface mechanically [123]. Jin et al. showed that AgNWs composite-based transparent electrodes with improved stability. They added an antioxidant which is a modified chitosan polymer, to the smooth AgNWs, which can protect the electrode from the perovskite side reactions. This cell showed a PCE of 7.9%; when compared to the reference device with the ITO electrode, its around 75% efficiency. With a large-scale device size of 50 m, it showed roughness of less than 10 nm with an excellent flat surface (Figure 9). The device shows improved stability without any adjustments even after 45 days with a temperature of 85 °C in sheet resistance [124].

In terms of device stability, by using fully solution-based conductive electrodes, which are transparent and found that these devices were shown good stability in ambient air for 30 days. These AgNWs were used as bottom electrodes in the ST-PSCs. ITO film AgNW film was deposited onto the ITO film, and the concentration of AgNWs was controlled by the spin coating speed [125]. Another method for lowering sheet resistance in ST-PSC has been reported, which involves spray coating AgNWs, which causes the density of AgNW electrodes to increase. The AgNW electrode was coated with a thin layer of ZnO nanoparticles. This device achieved an efficiency of around 7.30% with 23.3% AVT using an AgNW electrode. It was noticed that there was an improved PCE of 11.13% with the same AVT upon deposition of the ZnO layer [126]. Yang et al. reported room temperature deposition of AgNWs with spray coating with device yield efficiencies of up to 10.64% [127]. It was noticed that sheet resistance was found to be 11.86/sq with 88.6% transmittance at 550 nm and found to be comparable with the FTO, which is commercially available. The rigid substrate had an efficiency of 13.93%, and the flexible substrate had an efficiency of 11.23%. The device retained up to 94% of its initial efficiency even after 400 bending cycles with a 12.5 mm radius. According to the report, ZnO, which is doped with amorphous aluminium (a-AZO), showed good compact morphology when compared to c-AZO; hence a-AZO can assure AgNW. The conductivity of the composite electrode with a-AZO/AgNW/AZO could be maintained after the deposition of perovskites [128]. Due to the lack of consistency of silver with the perovskite, solution-processed AgNW has demonstrated an incredible ability to achieve much greater transparency over a broad range of wavelengths with a sheet resistance minimum. With solution-based AgNWs, an ST-PSC was reported by J. Brabec et al., they used AgNWs as a top electrode onto which they sandwiched a fine layer of zinc oxide nanoparticle between the electrode and ETL. Between the electrode and the ETL, this can ensure ohmic contact. In the absence of ZnO between $PC_{60}BM$ and AgNWs electrode, extracting the charges to the electrode efficiently would be difficult, owing to the high energy barrier between $PC_{60}BM$ and AgNWs (Figure 10). It showed a PCE of 8.49% with an AVT of 28.4% for the prepared semitransparent device [129].

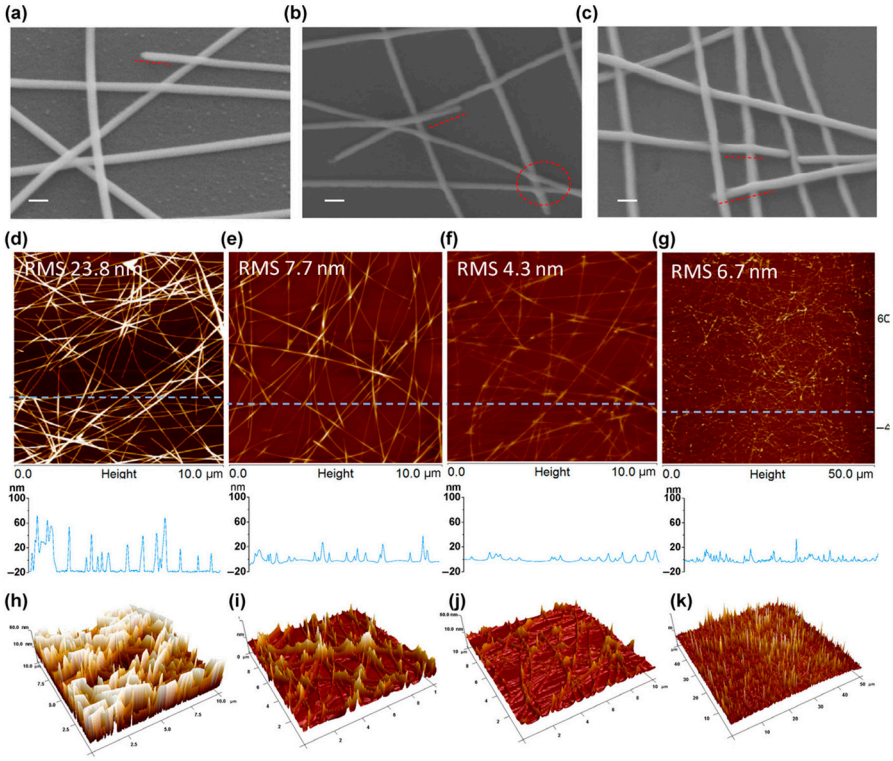

Figure 9. 30° tilt view SEM images of (**a**) 0.5 wt% overcoating of pristine AgNW networks and AgNW composite (**b**) and 1 wt% (**c**) Chi-AsA. The scale bar is 100 nm. Pristine AgNW networks' AFM height images and corresponding section profiles. (**d**) 0.5% Chi-AsA overcoated on AgNW composite. (**e**) 1 wt% Chi-AsA (**f**) and (**g**) scan size over 10 µm × 10 µm (**d**–**f**) and 50 µm × 50 µm (**g**). (**h**–**k**) AFM 3D images corresponding to (**d**–**g**) [124].

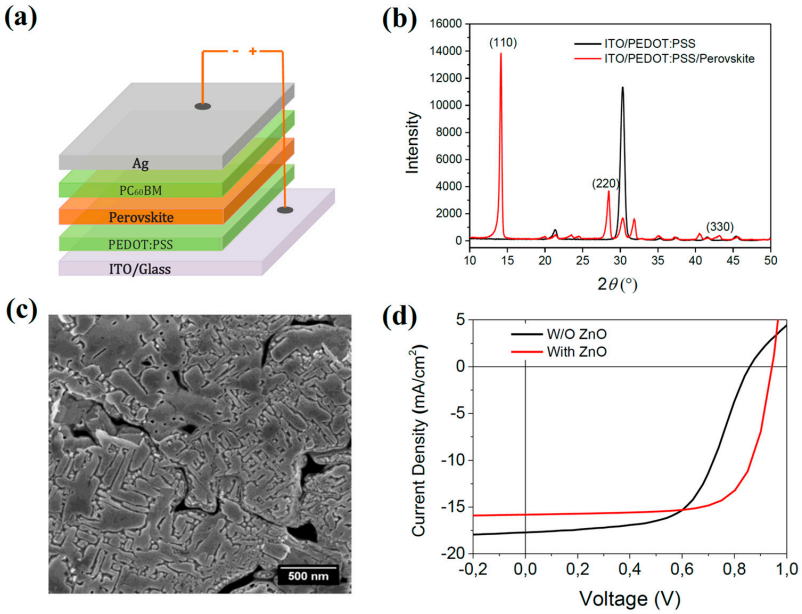

Figure 10. (**a**) The perovskite reference device's schematic architecture. (**b**) Perovskite crystals grown on PEDOT:PSS/ITO are shown in the XRD pattern (red line), and a control sample of the PEDOT:PSS-coated ITO substrate is shown for comparison (black line). (**c**) Top-view SEM image of the perovskite film in its growing state. (**d**) J-V curves of the two devices with and without a ZnO layer between the PC60BM and Ag top electrode [129].

Kang et al. demonstrated that semitransparent perovskite solar cells require transparent electrodes for achieving optical transparency (ST-PSCs). They used (IO:GT) a gallium and titanium-doped indium oxide to replace the ITO used in an inverted semitransparent device between ETL and the top electrode. The shallower work function of IO:GT (4.23 eV) compared to conventional ITO (4.69 eV) helps to prevent the Schottky barrier from forming and improve the transport of charge at the interface of the electron transport layer and cathode. By adopting IO:GT, the device reached maximum efficiency of 17.90% with an AVT of 21.9%, whereas in the absence of that, it showed 8.59%. Amongst all reported ST-PSCs data, this is the highest PCE achieved to date. A tandem solar cell by a four-terminal perovskite-perovskite device yielded a whopping PCE of 23.35% of these ST-PSCS were combined as a top cell. Additionally, the ST-PSCs' stability has been demonstrated that even after 77 days, roughly the device retained almost 96% of its initial PCE in an air environment, even in the absence of encapsulation, outperforming a device using a metal cathode. By looking into these results using IO:GT, there is cause for optimism in the area of inverted ST-PSCs [130].

Bolink et al. showed that Transparent conductive oxides (TCO) are typically deposited under severe conditions that frequently harm organic/soft under layers. By using a special industrial tool called pulsed laser deposition, they directly deposited ITO films on ST-vacuum deposited PSC successfully without disturbing the device pack. The PLD-deposited ITO films' morphological, electronic, and optical characteristics are enhanced. It is noticed that there exists a direct correlation between the pressure of the PLD chamber and the performance of the solar cell. The vacuum-assisted methods alone were used to make semitransparent PSCs with 78% FF and PCEs exceeding 18%. This result shows that efficient devices can be created by directly depositing TCO-based top electrodes without the use of shielding buffer layers [131].

4.8. Carbon Nanotubes

To calculate the resistance of the CNT network, contact resistance between carbon nanotubes and individual resistance of each carbon nanotube is required; this, in turn, depends on various factors such as synthetic methods, diameter, length, purity, and a few other factors. Multi-walled CNTs, which are free-standing, were reported by Kim et al., and sheets were put on the transparent top electrodes at room temperature (Figure 11). In comparison to metal electrodes, the cell showed PCE of around 1.5% and FF of around 58%, reduced leakage currents, and enhanced stability [132]. In 2014, the first attempts were made by Li et al., to fabricate a device based on an electrode made of carbon, where they laminated the CNT films on the perovskite layer and studied its device fabrication of a hole collector [133]. This investigation showed the creation of efficient electrodes without the use of costly metal deposition by vacuum.

In another study, a CNT which is single-walled was reported by Sakaguchi et al. as the top electrode, which showed a PCE of 11.8%. In this study, the cell was made without HTM, and in place of metal electrodes, SWNTs were used [134]. CNT was used by Jeon et al. as the cathode and anode to produce PSC, which is processable fully in solution. By doping *n*-type CNTs with $PC_{61}BM$, they claimed that CNTs soaked in P_3HT could serve as an anode and those soaked in $PC_{61}BM$ as a cathode [135]. The device's efficiency was 7.32%, while its flexibility was increased (Figure 12). Among single and multi-walled CNTs, Yoon et al. recently reported a CNT which is double-walled (DWNT), and this double-walled CNT device showed a PCE of 17.2%. Compared to previously reported CNTs, these double-walled CNTs showed higher conductivity and transparency. When these double-walled CNTs were doped with single-walled carbon nanotubes, the doping effect was reduced. The PSCs, which are of the inverted type, is made by using double-walled CNT films, which showed efficiencies of 15.6% prior to doping and were found to improve to 17.2% after Nitric acid and trifluoromethanesulfonic acid (TFMS) doping, respectively [136].

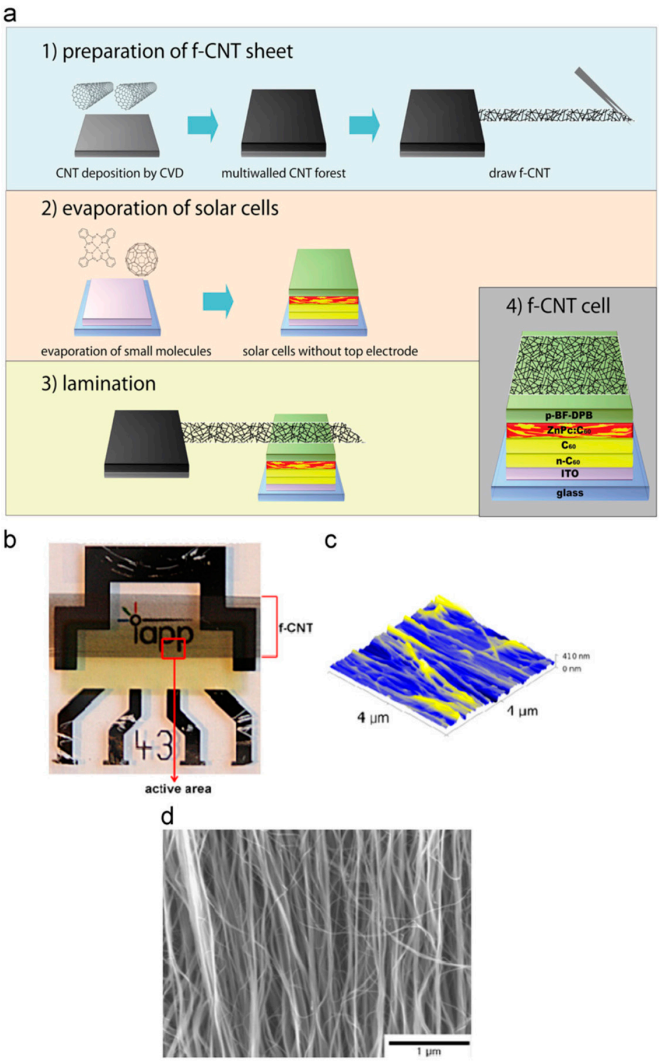

Figure 11. (**a**) Fabrication process f-CNT cell (**b**) a photograph of an f-CNT cell (**c**) AFM 4 × 4 µm (**d**) SEM image of f-CNT sheet on the top of solar cell [132].

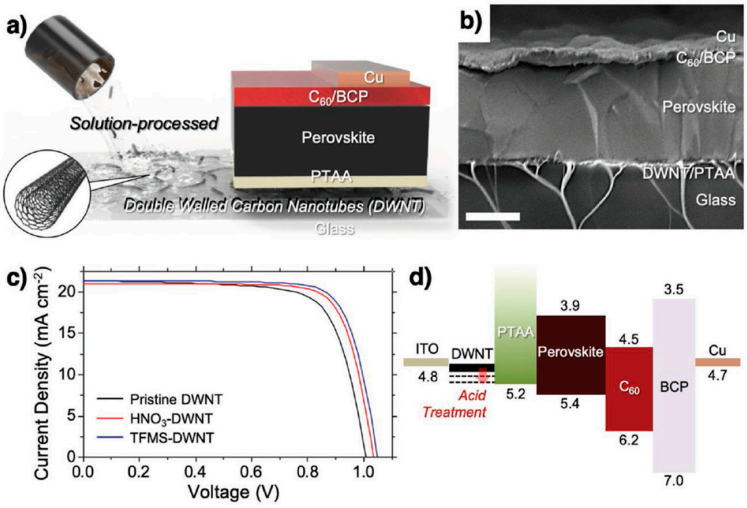

Figure 12. (**a**) a schematic representation of a PSC structure using transparent electrodes made of solution-processed DWNTs. (**b**) SEM image of a PSC in cross-section using the DWNT electrode (scale bar: 300 nm) (**c**) The J-V curves of the top-performing DWNT-PSCs with or without acid treatments (**d**) Energy level diagram of the PSCs fabricated in the current work [136].

On to the top electrode doping of MoO_3 in perovskite solar cells, carbon nanotubes serve multiple purposes by facilitating *p*-doping, advantageous such as enhanced hole mobility and proper energy level alignment. In order to reduce the sheet resistance of CNT electrodes without compromising the perovskite film Jasieniak et al. made, the ideal MoO_3 layer thickness (8 nm) is identified. A significantly better outcome compared to the earlier result of CNT doping with acid on the top electrode results in a reduction in sheet resistance of about one-third from its initial value. The carbon nanotube electrode's Fermi level is decreased by MoO_3 deposition, which enhances the electrode's ability to transfer holes and align energy levels. MoO_3 crystallises on the carbon nanotubes after being brushed with 2,2′,7,7′ Tetrakis[N,N-di(4-methoxyphenyl)amino]-9,9′-Spirobifluorene (spiro-MeOTAD), which improves hole collection. With a transmittance of about 60%, the ST-PSC, which are CNTs doped with MoO_3, showed PCE of 17.3% (at a wavelength of 1000 nm). Through computer simulations, these PSCs, when studied with silicon solar cells in tandem, showed their advantageous transparency in the infrared region. The expected device efficiency (23.7%) is greater than typical tandem solar cells made of indium-tin-oxide (23.0%) [137].

4.9. Graphene-Based Transparent Electrodes

Reports suggest that the materials containing graphene are unique in nature compared to FTO and ITO. In improving the performance of various solar devices, graphene gives a new path altogether due to its mechanical strength, highly chemically stable, comparatively cheaper, and improved transparency. Graphene is a suitable choice for electrodes which are transparent in ST-PSCs owing to its clean surface and enhanced conductivity [138]. There are few reports in ST-organic solar cells where graphene, which is single-layered, has been put onto P_3HT and PCBM as a top electrode [139]. With PEDOT:PSS solution and Au nanoparticles, the conductance of solar cells was altered, and the active layer and single-layer graphene work function were tuned. On the FTO glass substrate, the cell should contain TiO_2 as the electron transport layer, a layer which is photoactive, an HTL (spiro-OMeTAD/PEDOT:PSS), and a graphene layer. PEDOT:PSS will most likely improve the electrical conductivity of the graphene film in this case. The efficiency upon the usage of graphene electrode, the semitransparent device showed is 2.7%. When the device size increased from 6 to 50 mm^2, efficiency dropped to 2.3 (Figure 13) [138].

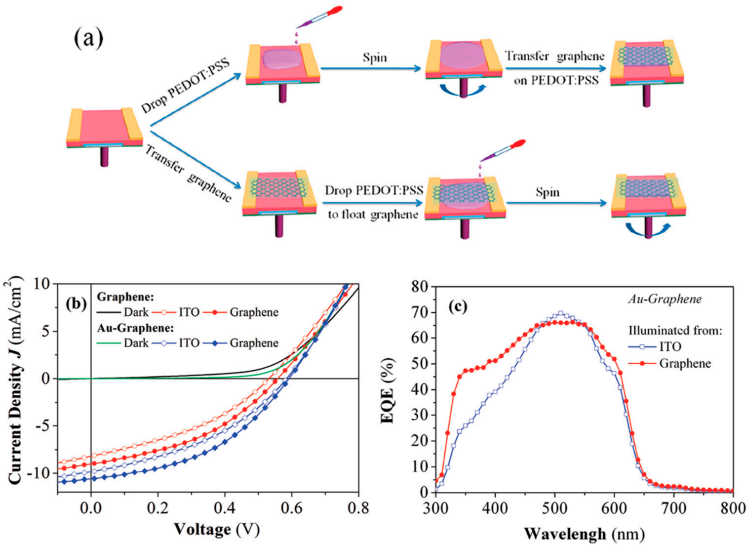

Figure 13. (**a**) Diagrammatic representation of the two methods for producing graphene/PEDOT:PSS top electrodes in organic solar cells. (**b**) Under a solar simulator, J-V characteristics of semi-transparent organic solar cells with a pure or Au-dopped graphene top electrode were measured on both sides. The devices' dark currents are also shown. (**c**) Organic solar cell with Au-doped graphene/PEDOT:PSS top electrode. EQE was measured from both sides. The results from the ITO and graphene sides are represented by the open and solid symbols, respectively [138].

In producing solar devices with graphene with multilayer stacking, the most suitable method is Chemical vapour deposition (CVD). During the lamination process, a fine layer of PEDOT:PSS was used as an adhesion layer to perovskite film, which also enhanced the conductivity of graphene. When illuminated from the FTO and Graphene sides, the devices showed approximately 12.02% and 11.62% PCE, respectively. Tran et al. recently published a flexible monolayer graphene in a large-scale and translucent bottom electrode. Plasma-assisted thermal chemical vapour deposition on a polymer substrate was used to directly synthesise graphene at 150 degrees Celsius without the usage of a transfer method. The top electrode was AZO/Ag/AZO, and the thickness of the cell around 300 nm showed a transmittance of 26% and PCE of 14.2%. The cell had the lowest sheet resistance of roughly 82/sq, the highest mechanical flexibility, and—perhaps most intriguingly—retained 90% of its initial efficiency even after 1000 bending cycles [140].

4.10. Plasmonic Au Nanorods

Etgar et al. showed that perovskite film could be thinned to achieve semitransparency, which has numerous advantages along with cost-effectiveness and lead reduction. However, this leads to limited light absorption. Thus, it is feasible to use metal nanostructures which are plasmonic to increase the electromagnetic field by trapping the incident light at the resonance peaks in order to prevent this loss. Here, non-harmful Au nanorods (NRs), whose resonance peak overlaps with the perovskite band gap, are applied on a thin (200 nm) ST perovskite layer. This device showed 13.7% of PCE with 27% AVT with 6% up from the reference cells. The trap density, nonradiative recombination, and defect density of these ST-PSCs, which are Au NR-treated, are further elucidated by space-charge restricted current, electrochemical impedance spectroscopy (EIS), and Mott-Schottky measurements (Figure 14). Additionally, Au NR implementation improves the solar cell's stability in ambient conditions. This demonstrates the use of the plasmonic effect to offset the light-harvesting of semitransparent perovskites [141].

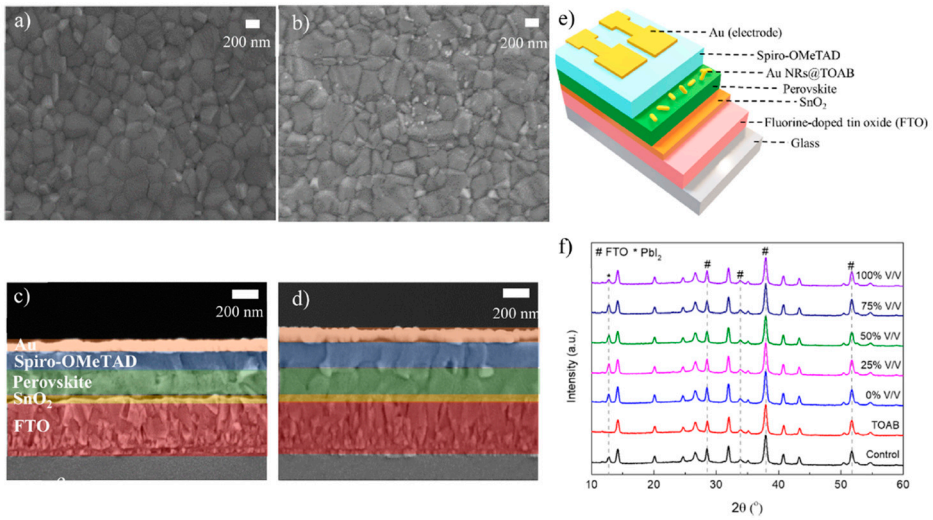

Figure 14. Perovskite without Au NR treatment in top-view and cross-sectional SEM images (**a**,**c**) and AuNR treatment with perovskite (**b**,**d**), (**e**) The PSC structure is shown schematically. (**f**) Perovskite film's XRD pattern as a function of Au NR treatment. 100% *v*/*v* denotes no dilution, while *v*/*v* indicates the degree of dilution [141].

As the transparent and conductive contact, ITO film is deposited onto the ST-PSCs. It is quite difficult to produce ITO layers of high quality as it requires processing at low temperatures below 50 °C. It is suggested in this study by Chen et al. that the transparent rear contact for a semitransparent device is a sandwiched structure of ITO/Ag/ITO and ITO/Cu/ITO formed at room temperature by sputtering. It is shown that by modifying the metal interlayer's thickness and surface shape, the AVT can be increased to 92.6%, and the

sheet resistance is less than 15.0. By utilising the good opto-electrical qualities, it is possible to increase the J_{sc} and FF of a semitransparent device with IAI and ICI rear contacts by around 1.0 mA/cm^2 and 10%, respectively. The PCE of ST-PSCs can be maintained above 13.0% even when the perovskite layer thickness is decreased to 488 nm. The PCE for a semitransparent perovskite solar cell lit from the IAI rear contact, and the glass substrate was around 9% and 15.8%, respectively [142].

4.11. Encapsulation of ST-PSC

Among all the drawbacks faced by the PSCs, poor device stability is one such prominent factor which remains the major challenge for commercial applications. Several independent factors, such as moisture, light illumination temperature, and oxygen, cause interfacial and perovskite-related degradations. Upon exposure to these factors, the photoactive medium gets destroyed, and the decomposition of halide-containing materials will degrade the pivotal layers of PSC severely, such as the metal electrodes. Hence, there is a need to protect the PSC from these factors; an effective and critical way of stabilisation was, in fact, found using encapsulation strategies and the development of new barriers, which will be helpful in protecting the sensitive part from the damage of the external factors.

In the case of ST-PSCs, degradation is more prominent because of ST top electrode is based on metal films which are ultrathin. To combat this issue, Riedl et al. demonstrated robust PSCs having a top electrode which is semitransparent, in which SnO_x surrounds the ultrathin Ag layers, which is grown by atomic layer deposition at low temperatures. Grown SnO_x acts as a permeation barrier, which is electrically conductive also, reduces the impact of moisture and which protects both the ultra-thin Ag electrode along with the perovskite film. This device showed PCE of greater than 11% and AVT of around 70% in the NIR region and 29% AVT in the visible region. Even after 4500 h of exposure to ambient temperatures and higher temperatures, this device showed good stability [143].

In another study, Chen et al. showed a self-encapsulated device without vacuum evaporating the metal electrode. In between two perovskite layers, they have added chlorobenzene, which helps in the interfusion of perovskite crystals which helps in obtaining light absorption and high crystallinity in laminated cells. This device showed PCE of 6.9% upon chlorobenzene treatment and showed excellent stability even after soaking in water for 24 h. Authors also suggested that this method is very effective in both making and cost-wise, and this would make way for commercial applications [144].

In the recent report of Park et al., they devised an ST PSC by utilising a lamination-assisted bifacial cation exchange technique involving a graphene electrode integrating with polyimide. After the lamination, they obtained high-quality ST-PSC via cation exchange reaction and showed PCE of 15.1%. Due to the presence of mechanically robust graphene electrodes and its chemically inert nature, this device showed good operational stability, moisture stability and mechanical durability [145].

In the case of ordinary PSCs, many other methods of encapsulating agents are used, such as flexible glass sheets, polymer nanocomposites and thin-film barriers, are used. Researchers need to focus more on customising these things when they need to be used in Semitransparent PSCs [146] (Table 1).

Among all photovoltaic technologies, the third-generation solar cells are best for BiPV applications based on their materials aspects, aesthetic colours and ease of fabrication on a flexible substrate. Among third-generation solar cells, perovskite devices are more encouraged towards BiPV based on their device efficiencies when compared to organic solar cells. The reason is that the perovskite solar cell efficiencies are very high than other technologies of this series. Therefore, one can expect more and more BiPV applications based on perovskite technology in the near future.

Table 1. Best efficiencies of flexible perovskite solar cells with different architecture.

Device Structure	V_{oc} (mV)	J_{sc} (mA/cm^2)	FF	Efficiency (%)	AVT (%)	Perovskite Thickness (nm)	Ref.
Glass/FTO/TiO_2/$MAPbI_3$/spiro-OMeTAD/MoO_3/Au (10 nm)/MoO_3	0.941	13.7	63	8.1	19	107	[82]
Glass/ITO/PEDOT:PSS/mixed-halideperovskite/PCBM/ZnO/AgNWs	1.1	15.2	75	12.6	17.3	-	[84]
FTO/TiO_2/PS/$MAPbI_3$/Spiro-OMeTAD/Au	0.950	19.2	64	11.7	36	400	[85]
Glass/FTO/c-TiO_2/m-TiO_2/$MAPbI_3$ grids/spiro-OMeTAD/Au (40 nm)	0.68	14.87	49	4.98	19	-	[86]
FTO/c-TiO_2/$CH_3NH_3PbI_{3-x}Cl_x$/spiro-OMeTAD/Ag SiO_2.HC (Honeycomb scaffold)	0.84	17.1	66	9.5	28		[87]
Glass/FTO/TiO_2/$FAPbI_3$ islands/spiro-OMeTAD/transparent laminated cathode	0.74	11.8	58	5.2	28.1	-	[88]
FTO/dual scaffold/ perovskite/Sprio-OMeTAD/Ag	-	-	-	12.32	23	100	[91]
Glass/FTO/c-TiO_2/AAO scaffold/$MAPbI_{3-x}Cl_x$ nanopillars/spiro-OMeTAD/MoO_x (5 nm)/ITO	0.99	15.87	74.53	11.72	33.4	350	[92]
n-type oxide/perovskite halide/p-type oxide	-	-	-	19.5	30		[94]
FTO/TiO_2/$MAPbI_3$/P3HT with additives/PEDOT:PSS/ITO planar sandwich solar cell	0.95	18	76	12.9	-	-	[106]
Glass/ITO or thin Au/PEDOT:PSS/$MAPbI_{3-x}Cl_x$/PCBM/b-MoO_3/Au (1 nm)/Ag(7 nm)/t-MoO_3/Alq_3	0.940	14.67	62.34	8.67	15.94	240	[112]
Glass/FTO/TiO_2/$MAPbI_3$ islands/PTAA/PEDOT:PSS/ITO	0.96	15.5	71.2	10.6	20.9	-	[113]
Glass/ITO/CuSCN/$MAPbI_3$/PC61BM/Bis-C60/Ag (20 nm)	1.06	13.0	73	10.73	13	240	[116]
Glass/FTO/TiO_2/$MAPbI_{3-x}Cl_x$ islands/$(CH_3(CH_2)_{17}SiCl_3)$/spiro-OMeTAD/Ni microgrid	0.75	13.82	59	6.1	38	-	[121]
ITO/AgNW/ITO	1.04	13.17	61.83	8.44	-	-	[125]
Glass/ITO/PEDOT:PSS/$MAPbI_{3-x}Cl_x$/PCBM/ZnO NPs/AgNWs	0.964	13.18	66.8	8.5	28.4	150	[129]
ITO/NiO_x/$FA_{0.87}Cs_{0.13}Pb(I_{0.87}Br_{0.13})_3$/PCBM/BCP/cathode	1.12	19.28	82.9	17.9	23.8		[130]
DWNT/poly(triaryl amine)(PTAA)[35 nm]/$MA0_{.6}FA_{0.4}PbI_{2.9}Br_{0.1}$ [450 nm]/C60 [20 nm]/bathocuproine (BCP) [6 nm]/Cu [50 nm]	1.05	21.4	77.1	17.2	-	-	[136]
glass/ITO/ZnO/P3HT:PCBM/PEDOT:PSS/graphene	0.612	9.66	44.15	2.61	-	-	[138]
FTO/SnO_2/perovskite/spiro-OMeTAD/Au	1.094	16.80	62.12	13.7	27	-	[141]

5. Conclusions

On the laboratory scale, PSCs have achieved almost 25% PCE, which brings the demand for the need of the technology to market levels. With their transparency, these PSCs could be introduced into the building ingredients to partially overcome the need in the energy requirements. In spite of the challenges still present, perovskite-based BIPVs still stand out due to their adaptability, flexibility and the large variety of capabilities that can address not only power generation but also the aesthetics and contentment of the building's exterior and interior. Hence it can be concluded that these PSCs can be seen in the buildings in the near future. These transparent devices give the freedom to install and replace the conventional materials on the buildings or on the windows. Although it is highly suggestible for the buildings, a few more aspects need to be addressed before going to the market level such as the stability of the device, toxic nature involved and environmental aspects. If these issues are addressed, we can see these devices installed in buildings in the near future.

Author Contributions: K.S.S. has contributed in this review for literature collection, drawings and writing the manuscript. P.R.M. has contributed literature collection. S.S. has involved in writing the review. L.G. has involved in supervision and manuscript writing. All authors have read and agreed to the published version of the manuscript.

Funding: This work was financially supported by the Department of Science and Technology under the Indo-Israel bilateral program (GAP-08; DST/INT/ISR/P-27/2020).

Acknowledgments: K. S. thanks DST for the Inspire fellowship. We thank the Director CSIR-IICT for their support (IICT/Pubs./2022/304).

Conflicts of Interest: The authors declare no conflict of interest.

References

1. Duzgun, B.; Koksal, M.A.; Bayindir, R. Assessing drivers of residential energy consumption in Turkey: 2000–2018. *Energy Sustain. Dev.* **2022**, *70*, 371–386. [CrossRef]
2. Kaygusuz, K. Energy and environmental issues relating to greenhouse gas emissions for sustainable development in Turkey. *Renew. Sustain. Energy Rev.* **2009**, *13*, 253–270. [CrossRef]

3. Jani, D.B.; Mishra, M.; Sahoo, P.K. A critical review on application of solar energy as renewable regeneration heat source in solid desiccant–vapor compression hybrid cooling system. *J. Build. Eng.* **2018**, *18*, 107–124. [CrossRef]
4. Garrett-Peltier, H. Green versus brown: Comparing the employment impacts of energy efficiency, renewable energy, and fossil fuels using an input-output model. *Econ. Model.* **2017**, *61*, 439–447. [CrossRef]
5. Omer, A.M. Renewable building energy systems and passive human comfort solutions. *Renew. Sustain. Energy Rev.* **2008**, *12*, 1562–1587. [CrossRef]
6. Hoffert, M.I.; Caldeira, K.; Benford, G.; Criswell, D.R.; Green, C.; Herzog, H.; Jain, A.K.; Kheshgi, H.S.; Lackner, K.S.; Lewis, J.S.; et al. Advanced technology paths to global climate stability: Energy for a greenhouse planet. *Science* **2002**, *298*, 981–987. [CrossRef]
7. Mrinalini, M.; Islavath, N.; Prasanthkumar, S.; Giribabu, L. Stipulating low production cost solar cells All set to retail. *Chem. Rec.* **2019**, *19*, 661–674. [CrossRef]
8. Trapani, K.; Millar, D.L. Proposing offshore photovoltaic (PV) technology to the energy mix of the Maltese islands. *Energy Convers. Manag.* **2013**, *67*, 18–26. [CrossRef]
9. Jäger-Waldau, A. Snapshot of photovoltaics—February 2019. *Energies* **2019**, *12*, 769. [CrossRef]
10. Chen, X.; Xiao, J.; Yuan, J.; Xiao, Z.; Gang, W. Application and performance analysis of 100% renewable energy systems serving low-density communities. *Renew. Energy* **2021**, *176*, 433–446. [CrossRef]
11. Biyik, E.; Araz, M.; Hepbasli, A.; Shahrestani, M.; Yao, R.; Shao, L.; Essah, E.; Oliveira, A.C.; Del Cano, T.; Rico, E.; et al. A method of strategic evaluation of energy performance of Building Integrated Photovoltaic in the urban context. *Int. J. Eng. Sci.* **2017**, *20*, 833–858. [CrossRef]
12. Available online: https://www.expertmarketresearch.com/reports/building-integrated-photovoltaics-market (accessed on 6 December 2022).
13. Sorgato, M.J.; Schneider, M.J.; Rüther, K. Technical and economic evaluation of thin-film CdTe building-integrated photovoltaics (BIPV) replacing façade and rooftop materials in office buildings in a warm and sunny climate. *Renew. Energy* **2018**, *118*, 84–98. [CrossRef]
14. Yang, S.; Cannavale, A.; Di Carlo, A.; Prasad, D.; Sproul, A.; Fiorito, F. Performance assessment of BIPV/T double-skin façade for various climate zones in Australia: Effects on energy consumption. *Sol. Energy* **2020**, *199*, 377–399. [CrossRef]
15. Available online: https://www.ntechresearch.com/news-posts/global-bipv-market/ (accessed on 6 December 2022).
16. Tripathy, M.; Sadhu, P.K.; Panda, S.K. A critical review on building integrated photovoltaic products and their applications. *Renew. Sustain. Energy Rev.* **2016**, *61*, 451–465. [CrossRef]
17. Bracquene, E.; Peeters, J.R.; Dewulf, W.; Duflou, J.R. Taking evolution into account in a parametric LCA model for PV panels. *Procedia CIRP* **2018**, *69*, 389–394. [CrossRef]
18. Wang, Y.; Boolchand, P.; Micoulaut, M. Glass structure, rigidity transitions and the intermediate phase in the Ge–As–Se ternary. *Europhys. Lett.* **2000**, *52*, 633. [CrossRef]
19. Fokaides, P.A.; Christoforou, E.A.; Kalogirou, S.A. Legislation driven scenarios based on recent construction advancements towards the achievement of nearly zero energy dwellings in the southern European country of Cyprus. *Energy* **2014**, *66*, 588–597. [CrossRef]
20. Ibn-Mohammed, T.; Koh, S.C.L.; Reaney, I.M.; Acquaye, A.; Schileo, G.; Mustapha, K.B.; Greenough, R. Perovskite solar cells: An integrated hybrid lifecycle assessment and review in comparison with other photovoltaic technologies. *Renew. Sustain. Energy Rev.* **2017**, *80*, 1321–1344. [CrossRef]
21. Ji, C.; Zhang, Z.; Masuda, T.; Kudo, Y.; Guo, L.J. Vivid-colored silicon solar panels with high efficiency and non-iridescent appearance. *Nano Scale Horiz.* **2019**, *4*, 874–880. [CrossRef]
22. Li, Z.; Wu, X.; Wu, W.; Gao, D.; Dong, H.; Huang, F.; Hu, X.; Jen, A.K.Y.; Zhu, Z. An effective and economical encapsulation method for trapping lead leakage in rigid and flexible perovskite photovoltaics. *Nano Energy* **2022**, *93*, 106853. [CrossRef]
23. Roy, A.; Ghosh, A.; Bhandari, S.; Sundaram, S.; Mallick, T.K. Perovskite solar cells for BIPV application: A review. *Buildings* **2020**, *10*, 129. [CrossRef]
24. Hegedus, S. Thin film solar modules: The low cost, high throughput and versatile alternative to Si wafers. *Prog. Photovolt. Res. Appl.* **2006**, *14*, 393–411. [CrossRef]
25. Ramanujam, J.; Bishop, D.M.; Todorov, T.K.; Gunawan, O.; Rath, J.; Nekovei, R.; Artegiani, E.; Romeo, A. Flexible CIGS, CdTe and a-Si: H based thin film solar cells: A review. *Prog. Mater. Sci.* **2020**, *110*, 100619. [CrossRef]
26. Sekitani, T.; Zschieschang, U.; Klauk, H.; Someya, T. Flexible organic transistors and circuits with extreme bending stability. *Nat. Mater.* **2010**, *9*, 1015–1022. [CrossRef]
27. Candelise, C.; Speirs, J.F.; Gross, R.J.K. Materials availability for thin film (TF) PV technologies development: A real concern? *Renew. Sustain. Energy Rev.* **2011**, *15*, 4972–4981. [CrossRef]
28. Wang, H. Progress in Thin Film Solar Cells Based on Cu_2ZnSnS_4. *Int. J. Photoenergy* **2011**, *2011*, 801292. [CrossRef]
29. Duvva, N.; Raptis, D.; Kumar, C.V.; Koukaras, E.N.; Giribabu, L.; Lianos, L. Design of diketopyrrolopyrrole chromophores applicable as sensitizers in dye-sensitized photovoltaic windows for green houses. *Dye. Pigment.* **2016**, *134*, 472–479. [CrossRef]
30. Lee, H.; Song, H.J. Current status and perspective of colored photovoltaic modules. *Wiley Interdiscip. Rev. Energy Environ.* **2021**, *10*, 403. [CrossRef]

31. Gambhir, A.; Sandwell, P.; Nelson, J. The future costs of OPV–A bottom-up model of material and manufacturing costs with uncertainty analysis. *Sol. Energy Mater. Sol. Cells* **2016**, *156*, 49–58. [CrossRef]
32. Espinosa, N.; Hösel, M.; Angmo, D.; Krebs, F.C. Highly conductive PEDOT: PSS electrode by simple film treatment with methanol for ITO-free polymer solar cells. *Energy Environ. Sci.* **2012**, *5*, 5117–5132. [CrossRef]
33. Giribabu, L.; Kanparthi, R.K.; Velkannan, V. Molecular engineering of sensitizers for dye-sensitized solar cell applications. *Chem. Rec.* **2012**, *12*, 306–328. [CrossRef] [PubMed]
34. Giribabu, L.; Kanparthi, R.K. Are porphyrins an alternative to ruthenium (II) sensitizers for dye-sensitized solar cells? *Curr. Sci.* **2013**, *104*, 847–855.
35. Yeoh, M.E.; Chan, K.Y. A review on semitransparent solar cells for real-life applications based on dye-sensitized technology. *IEEE J. Photovolt.* **2021**, *11*, 354–361. [CrossRef]
36. Gangadhar, P.S.; Jagadeesh, A.; George, A.S.; Reddy, G.; Prasanthkumar, S.; Soman, S.; Giribabu, L. An investigation into the origin of variations in photovoltaic performance using D–D–π–A and D–A–π–A triphenylimidazole dyes with a copper electrolyte. *Mol. Syst. Des. Eng.* **2021**, *6*, 779–789. [CrossRef]
37. Dessì, A.; Calamante, M.; Sinicropi, A.; Parisi, M.L.; Vesce, L.; Mariani, P.; Taheri, B.; Ciocca, M.; Di Carlo, A.; Zani, L.; et al. Thiazolo[5,4-d]thiazole-based organic sensitizers with improved spectral properties for application in greenhouse-integrated dye-sensitized solar cells. *Sustain. Energy Fuels* **2020**, *4*, 2309–2321. [CrossRef]
38. Roslan, N.; Ya'acob, M.E.; Radzi, M.A.M.; Hashimoto, Y.; Jamaludin, D.; Chen, G. Dye Sensitized Solar Cell (DSSC) greenhouse shading: New insights for solar radiation manipulation. *Renew. G Sustain. Energy Rev.* **2018**, *92*, 171–186. [CrossRef]
39. Gorjian, S.; Bousi, E.; Özdemir, O.E.; Trommsdorff, M.; Kumar, N.M.; Anand, A.; Kant, K.; Chopra, S.S. Progress and challenges of crop production and electricity generation in agrivoltaic systems using semi-transparent photovoltaic technology. *Renew. Sustain. Energy Rev.* **2022**, *158*, 112126. [CrossRef]
40. Theerthagiri, J.; Senthil, A.R.; Madhavan, J.; Maiyalagan, T. Recent progress in non-platinum counter electrode materials for dye-sensitized solar cells. *ChemElectroChem* **2015**, *2*, 928–945. [CrossRef]
41. Mohammadnezhad, M.; Selopal, G.S.; Wang, Z.M.; Stansfield, B.; Zhao, H.; Rosei, F. Role of carbon nanotubes to enhance the long-term stability of dye-sensitized solar cells. *ACS Photonics* **2020**, *7*, 653–664. [CrossRef]
42. Mastroianni, S.; Asghar, I.; Miettunen, K.; Halme, J.; Lanuti, A.; Brown, T.M.; Lund, P. Effect of electrolyte bleaching on the stability and performance of dye solar cells. *Phys. Chem. Chem. Phys.* **2014**, *16*, 6092–6100. [CrossRef]
43. Baxter, J.B. Commercialization of dye sensitized solar cells: Present status and future research needs to improve efficiency, stability, and manufacturing. *J. Vac. Sci. Technol. A Vac. Surf.* **2012**, *30*, 020801. [CrossRef]
44. Tumen-Ulzii, G.; Matsushima, T.; Adachi, T.C. Mini-review on efficiency and stability of perovskite solar cells with Spiro-OMeTAD hole transport layer: Recent progress and perspectives. *Energy Fuels* **2021**, *35*, 18915–18927. [CrossRef]
45. Tathavadekar, M.; Biswal, M.; Agarkar, S.; Giribabu, L.; Ogale, S.B. Electronically and Catalytically Functional Carbon Cloth as a Permeable and Flexible Counter Electrode for Dye Sensitized Solar Cell. *Electrochim. Acta* **2014**, *123*, 248–253. [CrossRef]
46. Arka, G.N.; Prasad, S.B.; Singh, S. Comprehensive study on dye sensitized solar cell in subsystem level to excel performance potential: A review. *Sol. Energy* **2021**, *226*, 192–213. [CrossRef]
47. Castro-Hermosa, S.; Yadav, S.K.; Vesce, L.; Guidobaldi, A.; Reale, A.; Di Carlo, A.; Brown, T.M. Stability issues pertaining large area perovskite and dye-sensitized solar cells and modules. *J. Phys. D Appl. Phys.* **2016**, *50*, 033001. [CrossRef]
48. Barichello, J.; Vesce, L.; Mariani, P.; Leonardi, E.; Braglia, R.; Di Carlo, A.; Canini, A. Stable semi-transparent dye-sensitized solar modules and panels for greenhouse application. *Energies* **2021**, *14*, 6393. [CrossRef]
49. Gokul, G.; Pradhan, S.C.; Soman, S. Dye-sensitized solar cells as potential candidate for indoor/diffused light harvesting applications: From BIPV to self-powered IoTs. In *Advances in Solar Energy Research*; Springer: Singapore, 2019; pp. 281–316. [CrossRef]
50. Rahdari, A.; Sheehy, B.; Khan, H.Z.; Braendle, U.; Rexhepi, G.; Sepasi, S. Exploring global retailers' corporate social responsibility performance. *Heliyon* **2020**, *6*, 04644. [CrossRef]
51. Moser, M.; Wadsworth, A.; Gasparini, N.; McCulloch, I. Challenges to the success of commercial organic photovoltaic products. *Adv. Energy Mater.* **2021**, *11*, 2100056. [CrossRef]
52. Rajeswari, R.; Mrinalini, M.; Prasanthkumar, S.; Giribabu, L. Emerging of inorganic hole-tranporting materials for perovskite solar cells. *Chem. Rec.* **2017**, *17*, 681–699. [CrossRef]
53. Babu, R.; Giribabu, L.; Singh, S.P. Recent advances in halide-based perovskite crystals and their optoelectronic applications. *Cry. Growth Des.* **2018**, *18*, 2645–2664. [CrossRef]
54. González-Carrero, S.; Galian, R.E.; Pérez-Prieto, J. Organometal halide perovskites: Bulk low-dimension materials and nanoparticles. *Part. Part. Syst. Charact.* **2015**, *32*, 709–720. [CrossRef]
55. Hoefler, S.F.; Trimmel, G.; Rath, T. Progress on lead-free metal halide perovskites for photovoltaic applications: A review. *Monatsh. Chem.* **2017**, *148*, 795–826. [CrossRef] [PubMed]
56. Rahmany, S.; Etgar, L. Semitransparent perovskite solar cells. *ACS Energy Lett.* **2020**, *5*, 1519–1531. [CrossRef]
57. Susrutha, B.; Giribabu, L.; Singh, S.P. Recent advances in flexible perovskite solar cells. *Chem. Commun.* **2015**, *51*, 14696–14707. [CrossRef] [PubMed]
58. Miyasaka, T. Perovskite photovoltaics: Rare functions of organo lead halide in solar cells and optoelectronic devices. *Chem. Lett.* **2015**, *44*, 720–729. [CrossRef]

59. Kumar, M.H.; Yantara, N.; Dharani, S.; Graetzel, M.; Mhaisalkar, S.; Boix, P.P.; Mathews, N. Flexible, low-temperature, solution processed ZnO-based perovskite solid state solar cells. *Chem. Commun.* **2013**, *49*, 11089–11091. [CrossRef]
60. Lu, H.; Krishna, A.; Zakeeruddin, S.M.; Grätzel, M.; Hagfeldt, A. Compositional and interface engineering of organic-inorganic lead halide perovskite solar cells. *iScience* **2020**, *23*, 101359. [CrossRef]
61. Azri, F.; Meftah, A.; Sengouga, N.; Meftah, A. Electron and hole transport layers optimization by numerical simulation of a perovskite solar cell. *Sol. Energy* **2019**, *181*, 372–378. [CrossRef]
62. Reddy, G.; Katakam, R.; Devulapally, K.; Jones, L.A.; Gaspera, E.D.; Updahyaya, H.M.; Islavath, N.; Giribabu, L. Ambient stable, hydrophobic, electrically conductive porphyrin hole-extracting materials for printable perovskite solar cells. *J. Mate. Chem. C* **2019**, *7*, 4702–4708. [CrossRef]
63. Williams, S.T.; Rajagopal, A.; Chueh, C.C.; Jen, A.K.Y. Current challenges and prospective research for upscaling hybrid perovskite photovoltaics. *J. Phys. Chem. Lett.* **2016**, *7*, 811–819. [CrossRef]
64. Mali, S.S.; Hong, C.K. p-i-n/n-i-p type planar hybrid structure of highly efficient perovskite solar cells towards improved air stability: Synthetic strategies and the role of p-type hole transport layer (HTL) and n-type electron transport layer (ETL) metal oxides. *Nanoscale* **2016**, *8*, 10528–10540. [CrossRef] [PubMed]
65. Schmidt, T.M.; Larsen-Olsen, T.T.; Carlé, J.E.; Angmo, D.; Krebs, F.C. Upscaling of perovskite solar cells: Fully ambient roll processing of flexible perovskite solar cells with printed back electrodes. *Adv. Energy Mater.* **2015**, *5*, 1500569. [CrossRef]
66. Wang, X.; Lu, X.; Liu, B.; Chen, D.; Tong, Y.; Shen, G. Flexible Energy-Storage Devices: Design Consideration and Recent Progress. *Adv. Mater.* **2014**, *26*, 4763–4782. [CrossRef] [PubMed]
67. Kim, D.H.; Muzzillo, C.P.; Tong, J.; Palmstrom, A.F.; Larson, B.W.; Choi, C.; Harvey, S.P.; Glynn, S.; Whitaker, J.B.; Zhang, F.; et al. Bimolecular additives improve wide-band-gap perovskites for efficient tandem solar cells with CIGS. *Joule* **2019**, *3*, 1734–1745. [CrossRef]
68. Mujahid, M.; Chen, C.; Zhang, J.; Li, C.; Duan, Y. Recent advances in semitransparent perovskite solar cells. *InfoMat* **2020**, *3*, 101–124. [CrossRef]
69. Xing, G.; Mathews, N.; Sun, S.; Lim, S.S.; Lam, Y.M.; Grätzel, M.; Mhaisalkar, S.; Sum, T.C. Long-Range Balanced Electron- and Hole-Transport Lengths in Organic-Inorganic CH3NH3PbI3. *Science* **2013**, *342*, 344–347. [CrossRef]
70. De Wolf, S.; Holovsky, J.; Moon, S.J.; Loper, P.; Niesen, B.; Ledinsky, M.; Haug, F.J.; Yum, J.H.; Ballif, C. Organometallic halide perovskites: Sharp optical absorption edge and its relation to photovoltaic performance. *J. Phys. Chem. Lett.* **2014**, *5*, 1035–1039. [CrossRef]
71. Yin, W.J.; Shi, T.; Yan, Y. Unique properties of halide perovskites as possible origins of the superior solar cell performance. *Adv. Mater.* **2014**, *26*, 4653–4658. [CrossRef]
72. Wu, Y.; Chen, W.; Chen, G.; Liu, L.; He, Z.; Liu, R. The impact of hybrid compositionalfilm/structure on organic–inorganic perovskite solar cells. *Nanomaterials* **2018**, *8*, 356. [CrossRef]
73. Kulkarni, S.A.; Baikie, T.; Boix, P.P.; Yantara, N.; Mathews, N.; Mhaisalkar, S. Band-gap tuning of lead halide perovskites using a sequential deposition process. *J. Mater. Chem.* **2014**, *2*, 9221–9225. [CrossRef]
74. Shi, B.; Duan, L.; Zhao, Y.; Luo, J.; Zhang, X. Semitransparent perovskite solar cells:from materials and devices to applications. *Adv. Mater.* **2020**, *32*, 1806474. [CrossRef] [PubMed]
75. Jeon, N.J.; Noh, J.H.; Kim, Y.C.; Yang, W.S.; Ryu, S.; Seok, S.I. Solvent engineering forhigh-performance inorganic–organic hybrid perovskite solar cells. *Nat. Mater.* **2014**, *13*, 897. [CrossRef] [PubMed]
76. Koh, T.M.; Wang, H.; Ng, Y.F.; Bruno, A.; Mhaisalkar, S.; Mathews, N. Halide perovskite solar cells for building integrated photovoltaics: Transforming building façades into power generators. *Adv. Mater.* **2022**, *34*, 2104661. [CrossRef] [PubMed]
77. Whitaker, J.B.; Kim, D.H.; Larson, B.W.; Zhang, F.; Berry, J.J.; Van Hest, M.F.; Zhu, K. Scalable slot-die coating of high performance perovskite solar cells. *Sustain. Energy Fuels* **2018**, *2*, 2442–2449. [CrossRef]
78. Dou, B.; Whitaker, J.B.; Bruening, K.; Moore, D.T.; Wheeler, L.M.; Ryter, J.; Breslin, N.J.; Berry, J.J.; Garner, S.M.; Barnes, F.S.; et al. Roll-to-roll printing of perovskitesolar cells. *ACS Energy Lett.* **2018**, *3*, 2558–2565. [CrossRef]
79. Park, M.; Kim, H.J.; Jeong, I.; Lee, J.; Lee, H.; Son, H.J.; Kim, D.E.; Ko, M.J. Mechanically recoverable and highly efficient perovskite solar cells: Investigation of intrinsicflexibility of organic–inorganic perovskite. *Adv. Energy Mater.* **2015**, *5*, 1501406. [CrossRef]
80. Yang, L.; Xiong, Q.; Li, Y.; Gao, P.; Xu, B.; Lin, H.; Li, X.; Miyasaka, T. Artemisinin-passivated mixed-cation perovskite films for durable flexible perovskite solar cells with over 21% efficiency *J. Mater. Chem. A* **2021**, *9*, 1574–1582. [CrossRef]
81. Finkenauer, B.P.; Gao, Y.; Wang, X.; Tian, Y.; Wei, Z.; Zhu, C.; Rokke, D.J.; Jin, L.; Meng, L.; Yang, Y.; et al. Mechanically robust and self-healable perovskite solar cells. *Cell Rep. Phys. Sci.* **2021**, *2*, 100320. [CrossRef]
82. Della Gaspera, E.; Peng, Y.; Hou, Q.; Spiccia, L.; Bach, U.; Jasieniak, J.J.; Cheng, Y.B. Ultra-thin high efficiency semitransparent perovskite solar cells. *Nano Energy* **2015**, *13*, 249–257. [CrossRef]
83. Rahmany, S.; Layani, M.; Magdassi, S.; Etgar, L. Fully functional semi-transparentperovskite solar cell fabricated in ambient air. *Sustain. Energy Fuels* **2017**, *1*, 2120–2127. [CrossRef]
84. Yeom, K.M.; Kim, S.U.; Woo, M.Y.; Noh, J.H.; Im, S.H. Recent Progress in Metal Halide Perovskite-Based Tandem Solar Cells. *Adv. Mater. Lett.* **2020**, *32*, 2002228. [CrossRef] [PubMed]
85. Chen, B.X.; Rao, H.S.; Chen, H.Y.; Li, W.G.; Kuang, D.B.; Su, C.Y. Ordered$macroporous CH_3NH_3PbI_3$ perovskite semitransparent film for high-performance solarcells. *J. Mater. Chem. A* **2016**, *4*, 15662–15669. [CrossRef]

86. Aharon, S.; Layani, M.; Cohen, B.E.; Shukrun, E.; Magdassi, S.; Etgar, L. Self-assembly of perovskite for fabrication of semitransparent perovskite solar cells. *Adv. Mater. Interfaces* **2015**, *2*, 1500118. [CrossRef]
87. Hörantner, M.T.; Zhang, W.; Saliba, M.; Wojciechowski, K.; Snaith, H.J. Templated microstructural growth of perovskite thin films via colloidal monolayer lithography. *Energy Environ. Sci.* **2015**, *8*, 2041–2047. [CrossRef]
88. Eperon, G.E.; Bryant, D.; Troughton, J.; Stranks, S.D.; Johnston, M.B.; Watson, T.; Worsley, D.A.; Snaith, H.J. Efficient, semitransparent neutral-colored solar cells based on microstructured formamidinium lead trihalide perovskite. *J. Phys. Chem. Lett.* **2015**, *6*, 129–138. [CrossRef]
89. Wang, Y.; Mahmoudi, T.; Yang, H.Y.; Bhat, K.S.; Yoo, J.Y.; Hahn, Y.B. Fully-ambient-processed mesoscopic semitransparent perovskite solar cells by islands-structure-MAPbI3-xClx-NiO composite and Al_2O_3/NiO interface engineering. *Nano Energy* **2018**, *49*, 59–66. [CrossRef]
90. Li, C.; Sleppy, J.; Dhasmana, N.; Soliman, M.; Tetard, L.; Thomas, J. A PCBM-assistedperovskite growth process to fabricate high efficiency semitransparent solar cells. *J. Mater. Chem. A* **2016**, *4*, 11648–11655. [CrossRef]
91. Xiao, S.; Chen, H.; Jiang, F.; Bai, Y.; Zhu, Z.; Zhang, T.; Zheng, X.; Qian, G.; Hu, C.; Zhou, Y.; et al. Hierarchical Dual-Scaffolds Enhance Charge Separation and Collection for High Efficiency Semitransparent Perovskite Solar Cells. *Adv. Mater. Interfaces* **2016**, *3*, 1600484. [CrossRef]
92. Kwon, H.C.; Kim, A.; Lee, H.; Lee, D.; Jeong, S.; Moon, J. Parallelized nanopillar perovskites for semitransparent solar cells using an anodized aluminum oxide scaffold. *Adv. Energy Mater.* **2016**, *6*, 1601055. [CrossRef]
93. Kwon, H.C.; Yang, W.; Lee, D.; Ahn, J.; Lee, E.; Ma, S.; Kim, K.; Yun, S.C.; Moon, J. Investigating recombination and charge carrier dynamics in a one-dimensional nano pillared perovskite absorber. *ACS Nano* **2018**, *12*, 4233–4245. [CrossRef]
94. Jung, E.H.; Jeon, N.J.; Park, E.Y.; Moon, C.S.; Shin, T.J.; Yang, T.Y.; Noh, J.H.; Seo, J. Efficient, stable and scalable perovskite solar cells using poly (3-hexylthiophene). *Nature* **2019**, *567*, 511–515. [CrossRef] [PubMed]
95. Alkhudhari, O.M.; Altujjar, A.; Mokhtar, M.Z.; Spencer, B.F.; Chen, Q.; Thomas, A.G.; Hodson, N.W.; Wang, X.; Hill, P.; Jacobs, J.; et al. High efficiency semitransparent perovskite solar cells containing 2D nanopore arrays deposited in a single step. *J. Mater. Chem.* **2022**, *10*, 10227–10241. [CrossRef]
96. Colsmann, A.; Puetz, A.; Bauer, A.; Hanisch, J.; Ahlswede, E.; Lemmer, U. Efficient semi-transparent organic solar cells with good transparency color perception and rendering properties. *Adv. Energy Mater.* **2011**, *1*, 599–603. [CrossRef]
97. Bauer, A.; Wahl, T.; Hanisch, J.; Ahlswede, E. ZnO: Al cathode for highly efficient, semitransparent 4% organic solar cells utilizing TiO x and aluminium interlayers. *Appl. Phys. Lett.* **2012**, *100*, 47. [CrossRef]
98. Qin, M.; Ma, J.; Ke, W.; Qin, P.; Lei, H.; Tao, H.; Zheng, X.; Xiong, L.; Liu, Q.; Chen, Z.; et al. Perovskite solar cells based on low-temperature processed indium oxide electronselective layers. *ACS Appl. Mater. Interfaces* **2016**, *8*, 8460–8466. [CrossRef] [PubMed]
99. Qin, P.L.; Lei, H.W.; Zheng, X.L.; Liu, Q.; Tao, H.; Yang, G.; Ke, W.J.; Xiong, L.B.; Qin, M.C.; Zhao, X.Z.; et al. Copper-Doped Chromium Oxide Hole-Transporting Layer for Perovskite Solar Cells: Interface Engineering and Performance Improvement. *Adv. Mater. Interfaces* **2016**, *3*, 1500799. [CrossRef]
100. Vosgueritchian, M.; Lipomi, D.J.; Bao, Z. Highly conductive and transparent PEDOT: PSS films with a fluorosurfactant for stretchable and flexible transparent electrodes. *Adv. Funct. Mater.* **2012**, *22*, 421–428. [CrossRef]
101. Lee, H.M.; Kang, S.B.; Chung, K.B.; Kim, H.K. Transparent and flexible amorphous In-Si-O films for flexible organic solar cells. *Appl. Phys. Lett.* **2013**, *102*, 021914. [CrossRef]
102. Cho, D.Y.; Kim, K.H.; Kim, T.W.; Noh, Y.J.; Na, S.I.; Chung, K.B.; Kim, H.K. Transparent and flexible amorphous InZnAlO films grown by roll-to-roll sputtering for acidic buffer-free flexible organic solar cells. *Org. Electron.* **2015**, *24*, 227–233. [CrossRef]
103. Choi, Y.Y.; Kang, S.J.; Kim, H.K. Rapid thermal annealing effect on the characteristics of $ZnSnO_3$ films prepared by RF magnetron sputtering. *Curr. Appl. Phys.* **2012**, *12*, S104–S107. [CrossRef]
104. Qin, P.; He, Q.; Ouyang, D.; Fang, G.; Choy, W.C.; Li, G. Transition metal oxides ashole-transporting materials in organic semiconductor and hybrid perovskite based solar cells. *Sci. China Chem.* **2017**, *60*, 472–489. [CrossRef]
105. Choi, S.; Potscavage Jr, W.J.; Kippelen, B. Area-scaling of organic solar cells. *J. Appl. Phys.* **2009**, *106*, 054507. [CrossRef]
106. Heo, J.H.; Han, H.J.; Lee, M.; Song, M.; Kim, D.H.; Im, S.H. Stable semi-transparent $CH_3NH_3PbI_3$ planar sandwich solar cells. *Energy Environ. Sci.* **2015**, *8*, 2922–2927. [CrossRef]
107. Löper, P.; Moon, S.J.; De Nicolas, S.M.; Niesen, B.; Ledinsky, M.; Nicolay, S.; Bailat, J.; Yum, J.H.; De Wolf, S.; Ballif, C. Organic–inorganic halide perovskite/crystalline siliconfour-terminal tandem solar cells. *Phys. Chem. Chem. Phys.* **2015**, *17*, 1619–1629. [CrossRef] [PubMed]
108. Kranz, L.; Abate, A.; Feurer, T.; Fu, F.; Avancini, E.; Löckinger, J.; Reinhard, P.; Zakeeruddin, S.M.; Grätzel, M.; Buecheler, S.; et al. High-efficiency polycrystallinethin film tandem solar cells. *J. Phys. Chem. Lett.* **2015**, *6*, 2676–2681. [CrossRef]
109. Fu, F.; Feurer, T.; Jäger, T.; Avancini, E.; Bissig, B.; Yoon, S.; Buecheler, S.; Tiwari, A.N. Low-temperature-processed efficient semi-transparent planar perovskite solar cells for bifacial and tandem applications. *Nat. Commun.* **2015**, *6*, 8932. [CrossRef]
110. Huang, J.; Li, G.; Yang, Y. A semi-transparent plastic solar cell fabricated by alamination process. *Adv. Mater.* **2008**, *20*, 415–419. [CrossRef]
111. Qin, P.L.; He, Q.; Chen, C.; Zheng, X.L.; Yang, G.; Tao, H.; Xiong, L.B.; Xiong, L.; Li, G.; Fang, G.J. High-Performance Rigid and Flexible Perovskite Solar Cells with Low-Temperature Solution-Processable Binary Metal Oxide Hole-Transporting Materials. *Sol. RRL* **2017**, *1*, 1700058. [CrossRef]

112. Ou, X.L.; Xu, M.; Feng, J.; Sun, H.B. Flexible and efficient ITO-free semi transparent perovskite solar cells. *Sol. Energy Mater. Sol. Cells* **2016**, *157*, 660–665. [CrossRef]
113. Heo, J.H.; Jang, M.H.; Lee, M.H.; Han, H.J.; Kang, M.G.; Lee, M.L.; Im, S.H. Efficiency enhancement of semi-transparent sandwich type $CH_3NH_3PbI_3$ perovskite solar cells with island morphology perovskite film by introduction of polystyrene passivation layer. *J. Mater. Chem. A* **2016**, *4*, 16324–16329. [CrossRef]
114. Sondheimer, E.H. The mean free path of electrons in metals. *Adv. Phys.* **2001**, *50*, 499–537. [CrossRef]
115. Kato, Y.; Ono, L.K.; Lee, M.V.; Wang, S.; Raga, S.R.; Qi, Y. Silver iodide formation inmethyl ammonium lead iodide perovskite solar cells with silver top electrodes. *Adv. Mater. Interfaces* **2015**, *2*, 1500195. [CrossRef]
116. Jung, J.W.; Chueh, C.C.; Jen, A.K.Y. High-performance semitransparent perovskite solar cells with 10% power conversion efficiency and 25% average visible transmittance based on transparent CuSCN as the hole-transporting material. *Adv. Energy Mater.* **2015**, *5*, 1500486. [CrossRef]
117. Tao, C.; Xie, G.; Liu, C.; Zhang, X.; Dong, W.; Meng, F.; Kong, X.; Shen, L.; Ruan, S.; Chen, W. Semitransparent inverted polymer solar cells with $MoO_3/Ag/MoO_3$ as transparent electrode. *Appl. Phys. Lett.* **2009**, *95*, 206. [CrossRef]
118. Wang, H.; Li, K.; Tao, Y.; Li, J.; Li, Y.; Gao, L.L.; Jin, G.Y.; Duan, Y. Smooth ZnO:Al-AgNWs composite electrode for flexible organic light-emitting device. *Nanoscale Res. Lett.* **2017**, *12*, 77. [CrossRef]
119. Chen, R.; Zhang, W.; Guan, X.; Raza, H.; Zhang, S.; Zhang, Y.; Troshin, P.A.; Kuklin, S.A.; Liu, Z.; Chen, W. Rear Electrode Materials for Perovskite Solar Cells. *Adv. Funct. Mater.* **2022**, *32*, 2200651. [CrossRef]
120. Roldan-Carmona, C.; Malinkiewicz, O.; Betancur, R.; Longo, G.; Momblona, C.; Jaramillo, F.; Camacho, L.; Bolink, H.J. High efficiency single-junction semitransparent perovskite solar cells. *Energy Environ. Sci.* **2014**, *7*, 2968–2973. [CrossRef]
121. Hörantner, M.T.; Nayak, P.K.; Mukhopadhyay, S.; Wojciechowski, K.; Beck, C.; McMeekin, D.; Kamino, B.; Eperon, G.E.; Snaith, H.J. Shunt-blocking layers for semitransparent perovskite solar cells. *Adv. Mater. Interfaces* **2016**, *3*, 1500837. [CrossRef]
122. Ye, T.; Jun, L.; Kun, L.; Hu, W.; Ping, C.; Ya-Hui, D.; Zheng, C.; Yun-Fei, L.; Hao-Ran, W.; Yu, D. Inkjet-printed Ag grid combined with Ag nanowires to form a transparent hybrid electrode for organic electronics. *Org. Electron.* **2017**, *41*, 179–185. [CrossRef]
123. Lee, J.; Lee, I.; Kim, T.S.; Lee, J.Y. Efficient welding of silver nanowire networks without post-processing. *Small* **2013**, *9*, 2887–2894. [CrossRef]
124. Jin, Y.; Sun, Y.; Wang, K.; Chen, Y.; Liang, Z.; Xu, Y.; Xiao, F. Long-term stable silvernanowire transparent composite as bottom electrode for perovskite solar cells. *Nano Res.* **2018**, *11*, 1998–2011. [CrossRef]
125. Kim, A.; Lee, H.; Kwon, H.C.; Jung, H.S.; Park, N.G.; Jeong, S.; Moon, J. Fully solution-processed transparent electrodes based on silver nanowire composites for perovskite solar cells. *Nanoscale* **2016**, *8*, 6308–6316. [CrossRef] [PubMed]
126. Sun, X.; Zha, W.; Lin, T.; Wei, J.; Ismail, I.; Wang, Z.; Lin, J.; Luo, Q.; Ding, C.; Zhang, L.; et al. Water-assisted formation of highly conductive silver nanowire electrode forall solution-processed semi-transparent perovskite and organic solar cells. *J. Mater. Sci.* **2020**, *55*, 14893–14906. [CrossRef]
127. Yang, K.; Li, F.; Zhang, J.; Veeramalai, C.P.; Guo, T. All-solution processed semi-transparent perovskite solar cells with silver nanowires electrode. *Nanotechnology* **2016**, *27*, 095202. [CrossRef] [PubMed]
128. Lee, E.; Ahn, J.; Kwon, H.C.; Ma, S.; Kim, K.; Yun, S.; Moon, J. All-Solution-Processed Silver Nanowire Window Electrode-Based Flexible Perovskite Solar Cells Enabled with Amorphous Metal Oxide Protection. *Adv. Energy Mater.* **2018**, *8*, 1702182. [CrossRef]
129. Guo, F.; Azimi, H.; Hou, Y.; Przybilla, T.; Hu, M.; Bronnbauer, C.; Langner, S.; Spiecker, E.; Forberich, K.; Brabec, C.J. High-performance semitransparent perovskite solarcells with solution-processed silver nanowires as top electrodes. *Nanoscale* **2015**, *7*, 1642–1649. [CrossRef]
130. Yoon, S.; Ha, H.U.; Seok, H.J.; Kim, H.K.; Kang, D.W. Highly Efficient and Reliable Semitransparent Perovskite Solar Cells via Top Electrode Engineering. *Adv. Funct. Mater.* **2022**, *32*, 2111760. [CrossRef]
131. Zanoni, K.P.; Paliwal, A.; Hernández-Fenollosa, M.A.; Repecaud, P.A.; Morales-Masis, M.; Bolink, H.J. ITO Top-Electrodes via Industrial-Scale PLD for Efficient Buffer-Layer-Free Semitransparent Perovskite Solar Cells. *Adv. Mater. Technol.* **2022**, *7*, 2101747. [CrossRef]
132. Kim, Y.H.; Sachse, C.; Zakhidov, A.A.; Meiss, J.; Zakhidov, A.A.; Müller-Meskamp, L.; Leo, K. Combined alternative electrodes for semi-transparent and ITO-free small molecule organic solar cells. *Sol. Energy Mater. Sol. Cells* **2012**, *96*, 244–250. [CrossRef]
133. Meng, F.; Zhou, Y.; Gao, L.; Li, Y.; Liu, A.; Zhang, C.; Fan, M.; Wei, G.; Ma, T. Environmental risks and strategies for the long-term stability of carbon-based perovskite solar cells. *Mater. Today Energy* **2021**, *19*, 100590. [CrossRef]
134. Sakaguchi, T.; Jeon, I.; Chiba, T.; Shawky, A.; Xiang, R.; Chiashi, S.; Kauppinen, E.I.; Park, N.G.; Matsuo, Y.; Maruyama, S. Non-doped and unsorted single-walled carbonnanotubes as carrier-selective, transparent, and conductive electrode for perovskite solar cells. *MRS Commun.* **2018**, *8*, 1058–1063. [CrossRef]
135. Jeon, I.; Seo, S.; Sato, Y.; Delacou, C.; Anisimov, A.; Suenaga, K.; Kauppinen, E.I.; Maruyama, S.; Matsuo, Y. Perovskite solar cells using carbon nanotubes both as cathode andas anode. *Phys. Chem. C* **2017**, *121*, 25743–25749. [CrossRef]
136. Jeon, I.; Yoon, J.; Kim, U.; Lee, C.; Xiang, R.; Shawky, A.; Xi, J.; Byeon, J.; Lee, H.M.; Choi, M.; et al. High-performance solution-processed double-walled carbonnanotube transparent electrode for perovskite solar cells. *Adv. Energy Mater.* **2019**, *9*, 1901204. [CrossRef]
137. Yu, J.C.; Li, B.; Dunn, C.J.; Yan, J.; Diroll, B.T.; Chesman, A.S.; Jasieniak, J.J. High-Performance and Stable Semi-Transparent Perovskite Solar Cells through Composition Engineering. *Adv. Sci.* **2022**, *9*, 2201487. [CrossRef]

138. Liu, Z.; Li, J.; Sun, Z.H.; Tai, G.; Lau, S.P.; Yan, F. The application of highly dopedsingle-layer graphene as the top electrodes of semitransparent organic solar cells. *ACS Nano* **2012**, *6*, 810–818. [CrossRef] [PubMed]
139. Liu, Z.; Lau, S.P.; Yan, F. Functionalized graphene and other two-dimensional materialsfor photovoltaic devices: Device design and processing. *Chem. Soc. Rev.* **2015**, *44*, 5638–5679. [CrossRef] [PubMed]
140. Tran, V.D.; Pammi, S.V.N.; Park, B.J.; Han, Y.; Jeon, C.; Yoon, S.G. Transfer-free graphene electrodes for super-flexible and semi-transparent perovskite solar cells fabricated under ambient air. *Nano Energy* **2019**, *65*, 104018. [CrossRef]
141. Lie, S.; Bruno, A.; Wong, L.H.; Etgar, L. Semitransparent Perovskite Solar Cells with >13% Efficiency and 27% Transperancy Using Plasmonic Au Nanorods. *ACS Appl. Mater. Interfaces* **2022**, *14*, 11339–11349. [CrossRef]
142. Chen, D.; Jiang, Y.; Sun, Z.; Huang, Y.; Yu, J.; Chen, T. ITO/Ag/ITO and ITO/Cu/ITO transparent rear contacts for semi-transparent perovskite solar cells. *Thin Solid Films* **2022**, *752*, 139252. [CrossRef]
143. Zhao, J.; Brinkmann, K.O.; Hu, T.; Pourdavoud, N.; Becker, T.; Gahlmann, T.; Heiderhoff, R.; Polywka, A.; Gorrn, P.; Chen, P.; et al. Self-Encapsulating thermostable and air-resilient semitransparent perovskite solar cells. *Adv. Eng. Mater.* **2017**, *7*, 1602599. [CrossRef]
144. Tan, L.; Liu, C.; Huag, Z.; Zhang, Y.; Chen, L.; Chen, Y. Self-encapsulated semi-transparent perovskite solar cells with water-soaked stability and metal-free electrode. *Org. Electron.* **2017**, *48*, 308–313. [CrossRef]
145. Jeong, G.; Koo, D.; Woo, J.-H.; Choi, Y.; Son, E.; Huang, F.; Kim, J.-Y.; Park, H. Highly efficient self-encapsulated flexible semitransparent perovskite solar cells via bifacial cation exchange. *ACS Appl. Mater. Interfaces* **2022**, *14*, 33297–33305. [CrossRef] [PubMed]
146. Sutherland, L.J.; Weerasingh, H.C.; Simon, G.P. A review on emerging barrier materials and encapsulation strategies for flexible perovskite and organic photovoltaics. *Adv. Eng. Mater.* **2021**, *11*, 2101383. [CrossRef]